Fall 2017

Electrical properties of metal/wse2structures

Zeel Rajiv Gandhi
New Jersey Institute of Technology

Copyright Warning & Restrictions

The copyright law of the United States (Title 17, United States Code) governs the making of photocopies or other reproductions of copyrighted material.

Under certain conditions specified in the law, libraries and archives are authorized to furnish a photocopy or other reproduction. One of these specified conditions is that the photocopy or reproduction is not to be "used for any purpose other than private study, scholarship, or research." If a, user makes a request for, or later uses, a photocopy or reproduction for purposes in excess of "fair use" that user may be liable for copyright infringement,

This institution reserves the right to refuse to accept a copying order if, in its judgment, fulfillment of the order would involve violation of copyright law.

Please Note: The author retains the copyright while the New Jersey Institute of Technology reserves the right to distribute this thesis or dissertation

Printing note: If you do not wish to print this page, then select "Pages from: first page # to: last page #" on the print dialog screen

ABSTRACT

ELECTRICAL PROPERTIES OF METAL/WSe_2 STRUCTURES

by
Zeel Rajiv Gandhi

The formation of low resistance metal contacts on two-Dimensional layer (2-D) of WSe_2 is a big challenge. In this research, a comparative study is presented on the electrical properties of metal/WSe_2 Schottky barrier diodes with various metals such as Au, In, Al, and Ga in the temperature range of 80K to 400K well within the domain of thermionic emission theory.

Topics covered here include the factors that determine the Schottky barrier height, the device capacitance, and its current-voltage (I-V) characteristics. I-V curves for different metals on WSe_2 are analyzed as function of temperature. Barrier height is determined from Au-nWSe_2 Schottky barrier diode.

This study provides a theoretical background for the selection of favourable metals on monolayer WSe_2.

ELECTRICAL PROPERTIES OF METAL/WSe_2STRUCTURES

by
Zeel Rajiv Gandhi

A Thesis
Submitted to the Faculty of
New Jersey Institute of Technology
in Partial Fulfillment of the Requirements for the Degree of
Master of Science in Materials Science and Engineering

Interdisciplinary Program in Materials Science and Engineering

December 2017

APPROVAL PAGE

ELECTRICAL PROPERTIES OF METAL/WSe_2 STRUCTURES

Zeel Rajiv Gandhi

Dr. N. M. Ravindra, Thesis Advisor — Date
Professor, Department of Physics, NJIT

Dr. Michael Jaffe, Committee Member — Date
Research Professor of Biomedical Engineering, NJIT

Dr. Oktay Gokce, Committee Member — Date
Senior University Lecturer of Physics, NJIT

Dr. Sagnik Basuray, Committee Member — Date
Assistant Professor of Chemical, Biological and Pharmaceutical Engineering, NJIT

BIOGRAPHICAL SKETCH

Author: Zeel Rajiv Gandhi

Degree: Master of Science

Date: December 2017

Undergraduate and Graduate Education:

- Master of Science in Materials Science and Engineering,
  New Jersey Institute of Technology, Newark, NJ, 2017

- Bachelor of Science in Applied Physics,
  St. Xavier's College, Ahmedabad, Gujarat, India, 2015

Major: Materials Science and Engineering

I would like to dedicate my work to:

My loving parents: Rajiv Gandhi and Reena Gandhi
For their unconditional love and support.
Thanks for being a constant motivational source for me.

ACKNOWLEDGMENT

I would first like to thank my thesis advisor, Dr. Nugehalli M. Ravindra, whose guidance and support from the beginning to the end of thesis enabled me to complete this work and I would be very thankful to him for giving me the privilege of working under his supervision. I would also like to acknowledge the committee members Dr. Sagnik Basuray, Dr. Michael Jaffe and Dr. Oktay Gokce for their valuable comments on this thesis and dedicating their precious time.

Thanks and love to my parents, Mr. Rajiv Gandhi and Mrs. Reena Gandhi, for providing me constant support, encouragement and always understanding me in my bad days whenever I had trouble with my thesis work.

At the end, thanks to all my friends, classmates and lab mates, I really enjoyed working with you all and whose encouragement played the greatest role.

TABLE OF CONTENTS

TABLE OF CONTENTS
(Continued)

LIST OF TABLES

LIST OF FIGURES

LIST OF FIGURES
(Continued)

LIST OF FIGURES
(Continued)

LIST OF FIGURES
(Continued)

CHAPTER 1

INTRODUCTION

In this thesis, the electrical properties of metal/WSe_2 structures are investigated. The details of this study are presented in nine chapters.

A brief introduction to the physical structure of WSe_2 is presented in Section 2.1. In Chapter 3, the structural and electronic properties of tungsten diselenide are summarized. The electronic band structure of $WSe_2$is presented in Section 3.2. The focus of Chapter 4 is on the electrical properties of WSe_2, in which the Sheet Resistance, Hall Effect, Electron and Hole mobilities and the temperature dependence of carrier mobilities are described. In Chapter 5, doping of WSe_2 is discussed.

Chapter 6 deals with the electronic and electrical properties of tungsten diselenide on different metals, wherein a description is given on the interface modeling and stability for monolayer (ML) WSe_2 on metal surfaces. Schottky barrier height is discussed in Section 6.6. In Section 6.7, the evolution of photovoltage from Schottky barriers, formed between different metals and WSe_2, is described. Further, the Current-Voltage (I-V) characteristics, Resistivity and Work Function are discussed in this Chapter. It focuses on the metal-semiconductor contacts describing the Ohmic and Schottky contacts, the energy band diagram for the contacts and the Junction Capacitance.

Chapter 7 describes the case study of four different metals namely, Al, Au, In and Ga on WSe_2. The I-V and C-V characteristics for these metals on WSe_2 are analyzed based on the experimental results in the literature.

In Chapter 8, the applications of WSe_2 are summarized, followed by conclusions in Chapter 9.

CHAPTER 2

OVERVIEW

Two-Dimensional materials, sometimes referred to as mono or single layer materials, are crystalline materials which consist of a single layer of atoms. Graphene was the first 2D material that was discovered in 2004; after that, about 700-2D materials have been predicted. Research on other 2D materials has taken place due to the zero bandgap of graphene that has limited its use as semiconductors, electrodes and device applications such as solar cells.

The discovery of graphene has directed scientists and researchers about new emerging physical properties when a bulk crystal of macroscopic dimension is thinned down to an atomic layer. Transition Metal Dichalcogenides (TMDCs) are such atomically thin semiconductors having the type MX_2; they have significant potential in electronic, optoelectronic and energy storage applications, which makes TMDCs more ideal materials over graphene.

In the past few years, there has been extensive research on WSe_2 based Schottky barrier diodes due to its less sensitivity to humidity, good stability, enhanced oxidation resistance and its marked anisotropy in most of its physical properties. Such properties make it an ideal material for evolutionary studies in Schottky barrier diodes.

2.1 Physical Properties of WSe_2

The transition metal dichalcogenides have a structure of MX_2, with ‘M’ representing transition metal atoms (such as W, Mo, Sc, etc) and ‘X’ as a chalcogen atom (Te, S, Se).They consist of a strongly bound X-M-X sandwich that is weakly stacked with other layers. The overall symmetry of TMDCs is rhombohedral or hexagonal, and the

metal atoms have octahedral or trigonal prismatic coordination. Figure 2.1 shows a hexagonal structure of monolayer TMDC.

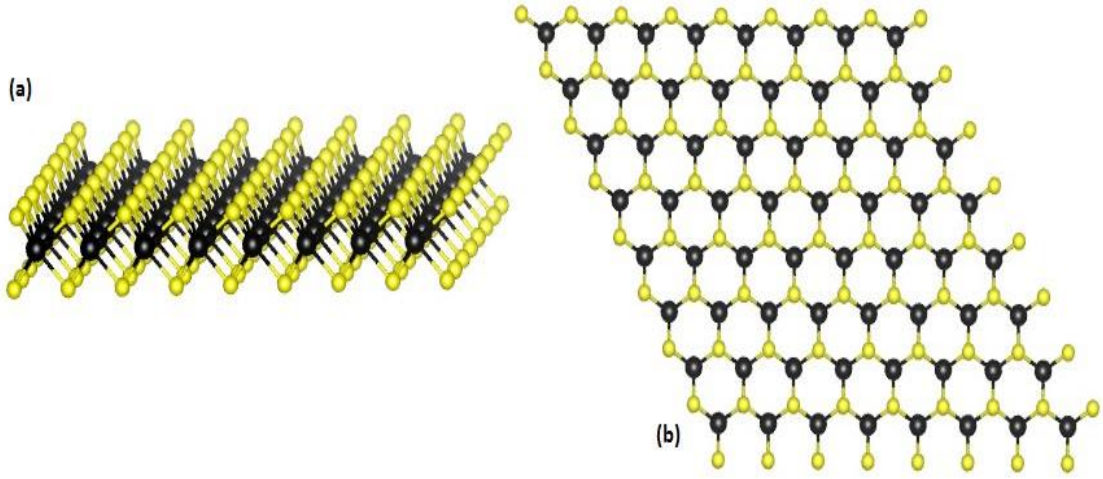

Figure 2.1(a) Hexagonal structure of monolayer TMDC. M atoms are in black and yellow shows the X atoms. (b) Top view of monolayer TMDC.

TMDCs such as $MoSe_2$, WS_2, WSe_2 and MoS_2 have a wide range of bandgaps that vary from indirect to direct in single layers, which allows their use as transistors, electroluminescent devices and photo-detectors. Although TMDCs have been studied for many years, recent advances in nanoscale material characterization and device fabrication have opened up new opportunities for 2-D layers of thin TMDCs in nanoelectronics and optoelectronics.

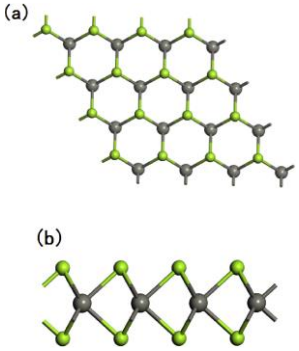

Figure 2.2 Schematic structure of monolayer WSe_2,(a) top view (b) side view. The gray and green balls represent W and Se atoms respectively.
Source: C. Yang, et al., (2017). Characters of group V and VII atoms doped WSe_2 monolayer, *J. Alloys and Compounds*, 699, 291-296.

Figure 2.2 depicts the crystal structure of monolayer WSe_2. 2H- WSe_2 belongs to the family of layered transition metal dichalcogenides(TMDCs) which display a wide variety of interesting physical properties and have thus been of continued interest for more than three decades.

WSe_2 is a very stable semiconductor in the group VI transition metal dichalcogenides. The compound has a hexagonal crystalline structure, in which every tungsten atom is covalently bonded to six selenium ligands in a trigonal prismatic coordinate sphere while each selenium is bonded to three tungsten atoms in a pyramidal like structure.

The W-Se bond has a length of 0.2526 nm, and the distance between each Se-atom in 0.334 nm. The inter layer distance between Se-W-Se bonds is ~0.7 nm. This is an experimental value that has been obtained for films prepared by Chemical Vapor Deposition (CVD) technique and mechanical exfoliation of bulk WSe_2 crystals. WSe_2 has a band gap of ~1.35 eV with a temperature dependence of the energy gap of -4.6×10^{-4} eV/K.

A few physical properties of WSe_2 are summarized in Table 2.1.

Table 2.1 Physical Properties of WSe_2

		Reference
Density	9.32 g/cm^3	[9]
Lattice parameter	a = 0.3297 nm, c = 1.298 nm	[9]
Molar Mass	341.6 g/mol	[9]
Melting Point	>1200 °C	[9]
Appearance	Grey to black solid	[26]
Solubility in water	insoluble	[9]
Odor	Odorless	[26]
Band Gap	~ 1eV (indirect, bulk) ~ 1.7 eV (direct, monolayer)	[26]

2.2 Preparation of WSe_2 Thin Films

There are various methods for synthesis of tungsten diselenide films. The techniques can be largely grouped into the categories of exfoliation, solution-phase synthesis, physical vapor deposition, chemical vapor deposition, and chalcogen substitution [27]. A case study on the soft selenization process, which comes under the group of physical vapor deposition (PVD) technique, is described here.

For the preparation of WSe_2 films by soft selenization process, tungsten films with varying thickness are deposited on chemically cleaned 5mm × 5mm quartz substrates by RF (radio frequency) magnetron sputtering method. The purity of W-target used is around 99.95%. Before the tungsten films are deposited onto the target, the target is pre-sputtered to remove extra residuals from its surface. The deposition rate of the film varies from 1.8 to 3.7 Å/s depending on the DC voltage used from batch to batch.

As the process name suggests, tungsten films are exposed to a selenium atmosphere. The selenium pellet used is 99.999% pure. In order to avoid extra deposition of selenium on tungsten than the required amount, the tungsten films and selenium pellet are sealed in an evacuated 30cm long silica glass vessel, with helium pressure of 10^{-3} Pa. These vessels are later placed in a pre-heated two-zone furnace with different temperature zones ranging from 543K to 1123K [22]. The selenium pellets are placed on the low temperature side, while the tungsten films are placed on the high temperature side. The time for selenization process is between 18h to 24h. After that time, the furnace is switched off and the vessels are taken out when it cools to room temperature, resulting in thin WSe_2 films. Figure 2.3 shows the temperature gradient of the two-zone furnace.

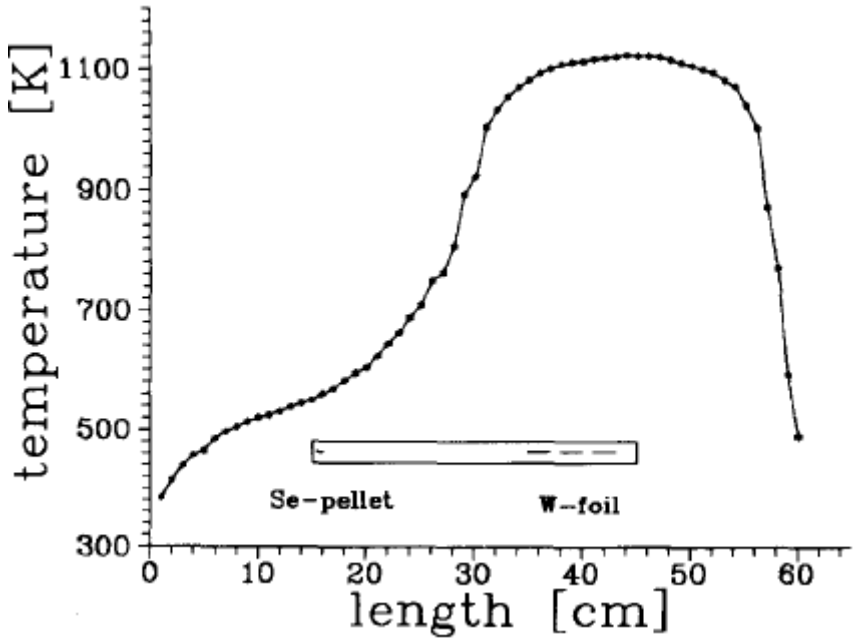

Figure 2.3 Temperature gradient of the two-zone furnace.
Source: A. Jager-Waldau and E. Bucher, (1991). WSe_2 Thin Films Prepared By Soft Selenization, *Thin Solid Films*, 200, 157-164.

CHAPTER 3

STRUCTURAL AND ELECTRONIC PROPERTIES OF WSe_2

In this chapter, a literature review of the structural and electronic properties of WSe_2 is presented. By knowing the electronic properties of a material, we can understand other properties that are exhibited by the material. It is necessary to know the band gap, lattice structure, optical gap transitions and lattice parameters of the material. Additionally, to know whether the material is a semiconductor or an insulator, we must know the band gap positions in the band structure.

3.1 Structural Properties of WSe_2

The crystal structure of 2H-WSe_2 belongs to the D^4_{6h} space group. Figure 3.1 shows the symmetric unit cell, which contains two formula units located in two adjacent hexagonal Se-W-Se layers. In each layer, the W atoms are coordinated in a trigonal prismatic arrangement.

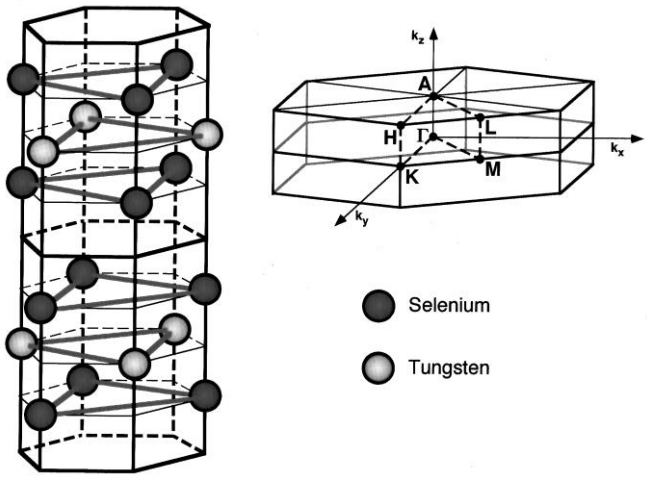

Figure 3.1 Hexagonal unit cell and Brillouin zone of 2H-WSe_2.
Source: Finteis Th., et al., (1997). Occupied and unoccupied electronic band structure of WSe_2, *Phy. Rev. B*, 55, 10400-10411.

Each single WSe_2sandwich layer as well as the surface is of threefold symmetry only, whereas the (infinite) crystal is of six-fold symmetry. Lattice constant ofWSe_2 is 3.28Å[11], while inter layer distance is correspondingly larger than other TMDCs due to large size of Se atom.

3.2 Electronic Band Structure of WSe_2

The band structure of WSe_2 exhibits both direct and indirect gaps. Direct gap exists at the K points of the Brillouin zone between the spin-orbit split valence band and doubly degenerate conduction band. On the other side, indirect gap is formed between a local conduction band minimum at a midpoint between Γ and K and valence band maximum at the Γ point. We can define symmetric lines and planes in the Brillouin zone. The Greek letters denote high symmetry points and the lines inside it, while the Roman letters denote those on the surface.

In 1977, WSe_2 was suggested to be a representative candidate for photovoltaic applications in electrochemical solar cells, for which conversion efficiencies up to 17% have been reported [11]. From the band structure calculations, bulk WSe_2 is an indirect-band-gap semiconductor; this is in agreement with optical absorption experiments. The size of the gap determined from the experiments was ~1.2 eV at 300K, which involves a transition from the Valence Band Maxima (VBM), formerly located at Γ, to the Conduction Band Minima (CBM) about halfway between Γ and K(as shown in Figure 3.1) [11].

In the monolayer emission spectra, it was noted that the indirect gap emission peak is virtually absent, which indicates that WSe_2 becomes a direct gap semiconductor when it is thinned to a single monolayer. For bulk WSe_2, the energy difference between the Γ and K points of the valence band was measured to be <80 meV by photoemission spectroscopy. For bilayer WSe_2, the difference between the

direct and indirect gaps is a measure of the energy separation between the conduction minimum at the K point and at the midpoint between Γ and K points. The energy separation in bilayer WSe_2 is found to be about 70 meV based on the photoluminescence results [10].

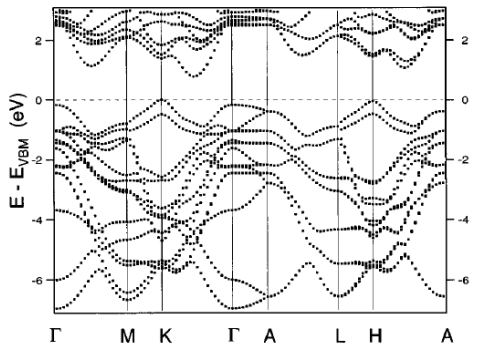

Figure 3.2 Theoretical (LDA) band structure for WSe_2. Energies are given relative to the valence-band maximum at the K point.
Source: Finteis Th., et al., (1997). Occupied and unoccupied electronic band structure of WSe_2, *Phy. Rev. B*, 55, 10400-10411.

Figure 3.2 shows the calculated band structures of WSe_2 along symmetry lines in the hexagonal Brillouin zone. For the symmetry labels, we used the notation of Miller and Love. For the calculation of the observed band structures in Figure 3.2, Th. Finteis *et al*. used a new local-density approximation (LDA) method, which yields agreement with the experimental results [11]. In contrast to the previous LDA calculations, no shape approximation to the potential or the charge density was made, and this is at the origin of the small but important differences between them and the present calculations provided by the researchers. The resulting band structure is shown in Figure 3.2.

These calculations were carried out by the experimentally determined structure parameters, i.e., W-to-Se-layer distance of z = 0.129 (in units of c), the topmost Eigen value at K being situated at ~80 meV below this value. This results in the valence-band maximum being located at the edge of the Brillouin zone (K) rather than at the centre (Γ) of it, with minimizing its effect on the rest of the band structure.

The VBM is now found to be as much as 170 meV higher in energy than the topmost state at Γ. Here, an exclusively W $5d_{xy,x^2-y^2}$ character is observed for the two topmost bands at K, which leads to a very weak dispersion that is perpendicular to the WSe_2 sheets. Therefore, the valence-band edge now appears to be of much more two-dimensional nature [11].

Different papers have different values used for determining the band structure, and so the band structure varies. Very recently, another band calculation using the linear muffin-tin orbital method was carried out where the observed value of z = 0.125 and 18 meV difference between Γ and K.

However, recently studied Scanning Tunnelling Spectroscopy (STS) suggests that the Q-valley is about 80 meV below the K-valley in the Conduction Band (CB) of monolayer WSe_2, which indicates an indirect quasi-particle gap [28]. Whether the optical gap in monolayer WSe_2 is indirect or not still remains unclear. Current advances in research says that, both the direct and indirect gap of WSe_2 are externally influenced by strain. The indirect gap energy is pushed away from the initial value (that is, the energy value increases) or is brought closer in the direct gap by strain; the exciton population participating in the direct gap recombination will be affected by the presence of nearly degenerated indirect gap, leading to changes in the energy and intensity of direct exciton photoluminescence [28].

3.3 Effect of Temperature on Energy Gap of Monolayer WSe_2

Band gap engineering is an important field in electronics. The ability to control the band gap of a semiconductor helps in creating desirable electrical and optical properties of the semiconductor material. The energy gap of a semiconductor is directly dependent on temperature. Due to the increase in thermal energy, there is an increase in atomic spacing caused by the increase in lattice vibrations. This increase in

atomic spacing decreases the potential seen by the electrons in the material, reducing the size of the energy gap. Thus, in semiconductors, the energy gap decreases with increase in temperature. Surface doping can also control the band structure of WSe_2. The temperature dependence of the energy gap of WSe_2 is determined by a direct replacement equation (Equation 3.1) of Varshini's equation, as formulated by O'Donnell [23]. This equation is found to have better results compared to other theoretical approaches.

$$E_g(T) = E_g(0) - S\langle\hbar\omega\rangle [(\coth \langle\hbar\omega\rangle / 2kT) - 1] \quad (3.1)$$

In Equation (3.1), $E_g(0)$ is the band gap at 0K, S is a dimensionless coupling constant and $\langle\hbar\omega\rangle$ is an average phonon energy. Fitting parameters, based on Equation (3.1), are tabulated in Table 3.1 for tungsten diselenide.

Table 3.1 Fitting Parameters of Energy Gap for ML WSe_2

Material	**$E_g(0)$ (eV)**	**S**	**$\langle\hbar\omega\rangle$ (meV)**	**Reference**
WSe_2	1.742	2.06	1.50	23

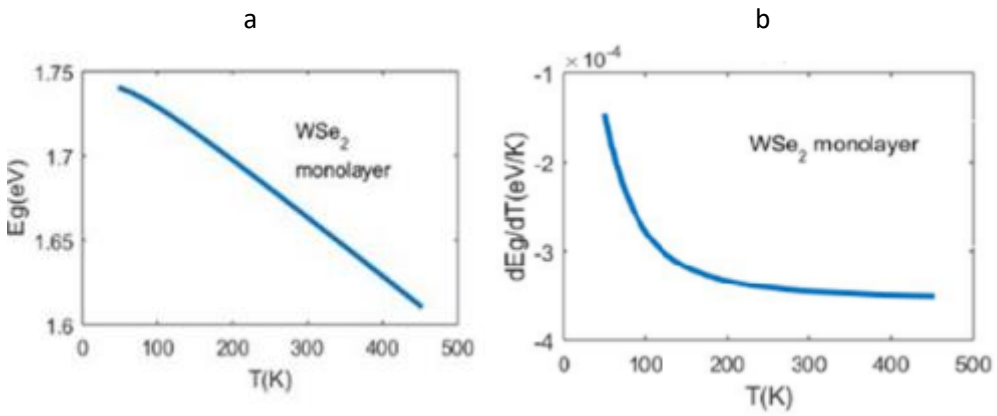

Figure 3.3 (a) Temperature dependence of the energy gap of monolayer WSe_2. (b) $\frac{dE_g}{dt}$ of monolayer WSe_2.
Source: https://ecee.colorado.edu/~bart/book/book

Figure 3.3(a) shows the variation in band gap with temperature and Figure 3.3(b) depicts the $\frac{dE_g}{dt}$ plot for monolayer WSe_2. From Figure 3.3 it is clear that with increase in temperature the energy gap decreases, which is normally the case for most semiconductors. It also shows that the $\frac{dE_g}{dt}$ is non linear with temperature and decreases with increase in temperature.

CHAPTER 4

ELECTRICAL PROPERTIES OF SEMICONDUCTORS

4.1 Sheet Resistance

The measure of resistance of thin films in two-dimensions with uniform thickness is normally called Sheet resistance. As the name indicates, it is implied that the current is along the plane of the sheet and not perpendicular to it.

It is generally used for characterizing materials that are made by semiconductor doping, metal deposition, glass coating and resistive paste printing. The major advantage of sheet resistance over resistance or resistivity is that, it is directly measured using the four-point probe measurement. In addition to it, we can compare electrical properties of devices that are significantly different in size, because sheet resistance is invariable under scaling.

For a regular 3-D conductor, Resistance R is given by Equation 4.1, where ρ is the resistivity (ohm·m), A is the cross-section area(A in terms of W(width) and t(thickness of the wafer) as shown in Figure 4.1), and L is the length.[12]

$$R = \rho \frac{L}{A} = \rho \frac{L}{Wt} \tag{4.1}$$

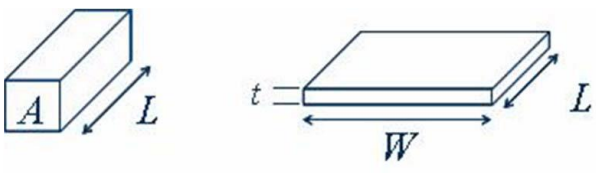

Figure 4.1 A regular 3-D conductor.

Source:astro1.panet.utoledo.edu/~relling2/.../20111025_lecture_4.2_phys4580.6280.pdf

The units of sheet resistance is Ohms, but is also expressed in terms of ohms per square. It is denoted by the following Equation 4.2.

$$R = \frac{\rho}{t}\frac{L}{W} = R_s\frac{L}{W} \quad (4.2)$$

As an example, a square sheet with an R_s of 100 ohm/sq. has a resistance of 100 ohms., regardless of the size of the square.

4.2 Hall Effect

Hall effect is the most common method that is used to characterize the electrical properties of semiconductors or conductors. We can determine the type of semiconductor (p or n type). Figure 4.2 illustrates the geometrical set up for Hall effect experiment. Here, a conducting slab with length L is placed in the x direction, width w in the y direction and thickness t in the z direction. The charge carrier in the slab is assumed to be charge q.

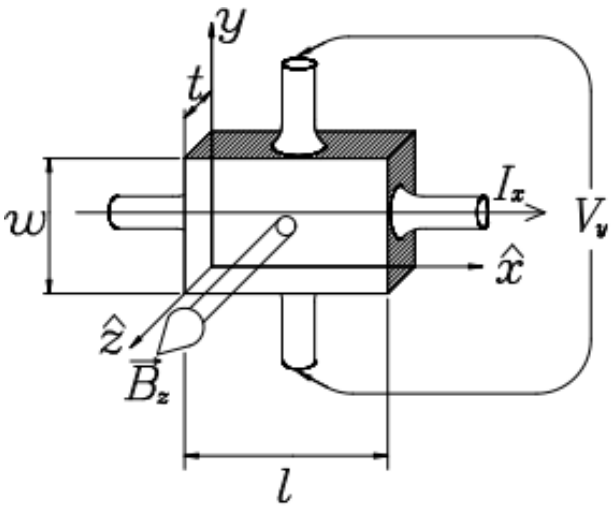

Figure 4.2 Geometry of fields and sample in Hall effect experiment
Source: courses.washington.edu/phys431/hall_effect/hall_effect.pdf

$$I_x = J_x wt = nqv_x wt \quad (4.3)$$

Equation 4.3 shows that current I_x is the product of current density (J_x) and the cross sectional area of the conductor (wt); where current density is also a product of charge density (nq) and drift velocity v_x.[12]

The Hall field (in the y direction) is written by the equation given below:

$$E_y = v_x B_z \tag{4.4}$$

In this experiment, we measure the potential difference across the sample, i.e. the Hall voltage V_H which is related to the Hall field (E_y) by the relation as shown in equation 4.5.

$$V_H = -\int_0^w E_y dy = - E_y w \tag{4.5}$$

On equating Equations 4.3, 4.4 and 4.5, we get

$$V_H = -\left(\frac{1}{nq}\right)\frac{I_x B_z}{t} \tag{4.6}$$

In equation 4.6, the first term on right hand side is known as the Hall coefficient:

$$R_H = \frac{1}{nq} \tag{4.7}$$

The Hall coefficient is positive if the charge carriers are positive, and will be negative if the charge carriers are negative. The SI unit of Hall coefficient is m^3/A-s or m^3/C.

4.3 Electron and Hole Mobilities

Mobility is defined as the drift velocity per unit electric field. With the application of electric field, electrons get drifted. This drift velocity of electrons per unit electric field is known as electron mobility, which is a measure of the effect of electric field on the motion of electrons. In semiconductors, there is relatively more quantity of holes, and thus the so called hole mobility.

On applying electric field E across a piece of material, the electrons move with an average velocity called the drift velocity, denoted as v_d. Then the electron mobility μ is defined as

$$v_d = \mu E \tag{4.8}$$

This further implies as:

$$\mu = \frac{v_d}{E} \tag{4.9}$$

The electron mobility is always specified in units of $cm^2/(V*s)$. The SI unit of mobility is $m^2/(V*s)$. The hole mobility is expressed with the same equation as electron mobility.

4.3.1 Temperature Dependence of Mobilities

Figure 4.3 shows the field effect mobilities as a function of temperature on the p and n side.

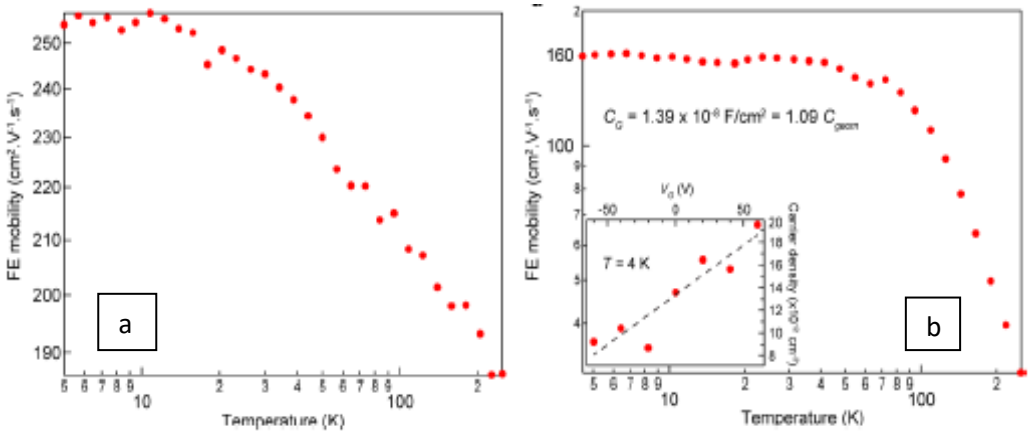

Figure 4.3 The field-effect mobilities as a function of temperature (a) on the p-side and (b) n-side. Inset of (b) carrier density on the n-side, measured using the Hall effect. The extracted back-gate capacitance is indicated in the figure.

Source: Adrien Allain and Andras Kis, (2014). Electron and Hole Mobilities in Single-Layer WSe_2, *ACS Nano*, 8, 7180-7185.

CHAPTER 5

DOPING OF WSe_2

Doping is a process in which impurities are introduced into the pure semiconductor crystal for the purpose of modulating its electrical properties. Basically, the doped material is known as an extrinsic semiconductor. There are two types of doping: n- and p-type doping. The type of doping that needs to be carried out depends on the number of outer electrons in the lattice structure of the semiconductor crystal. Elements with three valence electrons are used for p-type doping and the one with five valence electrons are used for n-type doping. After detailed research done by Zhao et al., it was concluded that group V elements facilitate p-type doping and group VII elements result in an n-type doping for WSe_2 structures [21]. Figure 5.1 shows the electronic band structure in doped semiconductors.

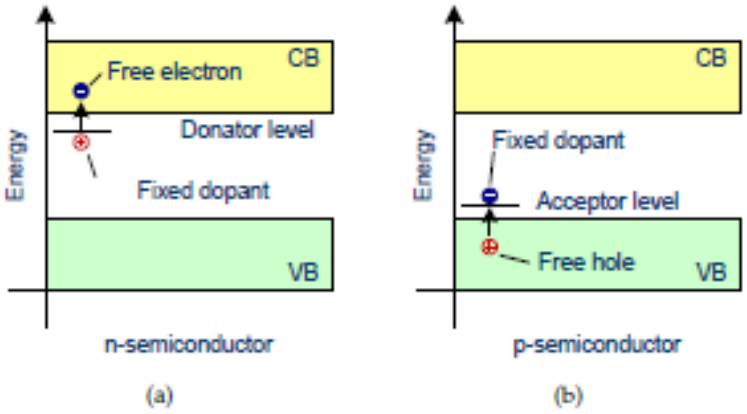

Figure 5.1 Band model of (a) n-type and (b) p-type semiconductors.
Source: https://www.halbleiter.org/en/fundamentals/doping/

In n-doped semiconductors, the electron in the crystal is weekly bound and so it can be moved to the conduction band with less energy. Commonly, in this type of doping, there is a donor energy level (as shown in Figure 5.1) near the conduction band. The band gap is very small. For p-doped semiconductors, there is an acceptor

energy level near the valence band. A hole is available in the valence band which is occupied by an electron from the dopant at a low energy.

5.1 p-doping of WSe_2

p-doping is done by chemisorption of NO_2 on WSe_2 at temperature of 150 °C at set reaction time of 4 to 12 h. This doping process leads to a five orders of reduction in magnitude in contact resistance between WSe_2 and Pd metal, resulting in a degenerate doping concentration (n_i^2) of 1.6×10^{19} cm^{-3} [16].

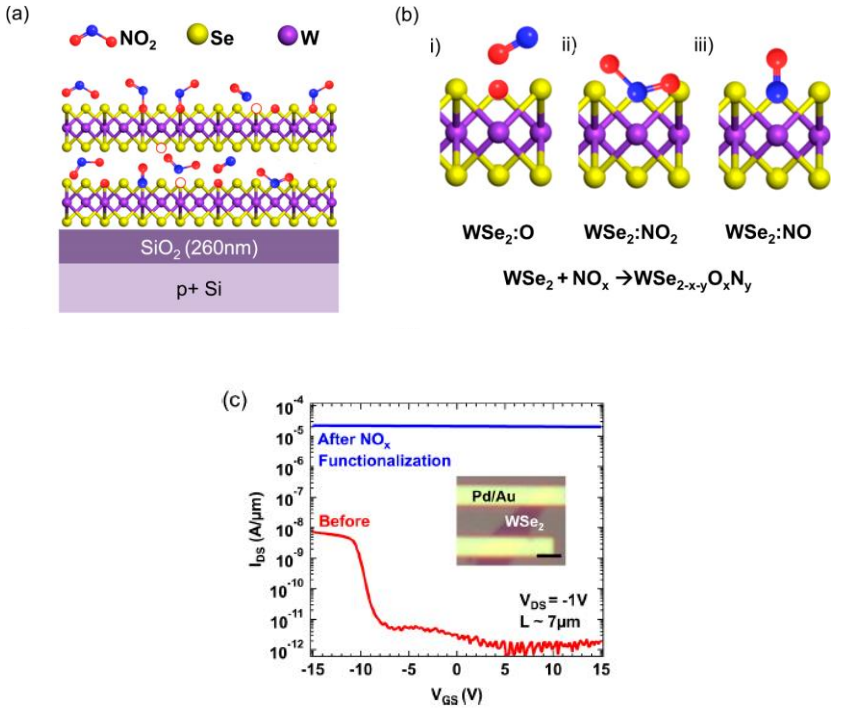

Figure 5.2 (a) Schematic of NO_x chemisorption process at the WSe_2 bulk and surface.(b) Proposed specific NO_x chemisorption at the selenium vacancy sites can lead to three distinct configurations:(i) WSe_2:O, (ii) WSe_2:NO_2, (iii) WSe_2:NO. (c) I_{DS} -V_{GS} of before and afterNO_2 treated devices. Inset: Optical microscopy of fabricated device using Pd/Au contacts; scale bar is 2 μm.
Source: Zhao Peida, et al., (2014). Air Stable p-Doping of WSe_2 by Covalent Functionalization, *ACS Nano*, 8, 10808-10814.

NO_2 has a strong oxidizing nature which leads to an induced NO_x chemisorption process on the WSe_2 surface and bulk defect sites (e.g. selenium vacancies), which forms stable electron withdrawing $WSe_{2-x-y}O_xN_y$ species that lead to p-doping (as seen in Figure 5.2(a,b). Figure 5.2 (b) shows three most likely

scenarios: (i) direct W oxidation resulting from the O of NO_2 which occupies a Se vacancy, following the thermal dissociation ofNO_2 and desorption of NO; (ii) the alternate NO_2 absorption configuration with N directly bonding to W at the Se vacancy site and (iii) here N of NO (where NO is formed through dissociation of NO_2) is covalently bonded to W.

In Figure 5.2(c), the transfer characteristics of p-doped devices are measured before and after the induced NO_x chemisorption process. Here, the thickness of the WSe_2 flake used is ~5 nm. After the chemisorption process, a dramatic change in the p-FET characteristic is found. The value of $I_{on}$is about 10^{-8} A/μm which later increases by about 1000 times [16]. Due to the hole doping, the Fermi level(E_F) moves closer to the Valence band edge (E_V).

5.2 n-doping of WSe_2

The method of n-doping of WSe_2 is done by depositing thin films of silicon nitride on the surface of WSe_2 by plasma enhanced chemical vapor deposition (PECVD). Silicon nitride, that is grown by PECVD process, contains a high density of positive charge centers which originate from $^{+}Si{\equiv}N_3$ dangling bonds known as K^+ centers, as shown in Figure 5.3(a). In Figure 5.3(b), it is observed that a strong field-induced electron doping of WSe_2 is carried out by SiN_x coating. The electron sheet density can be varied as per need. This allows us to fabricate stable n-type WSe_2 transistors with range of properties as required by the user.

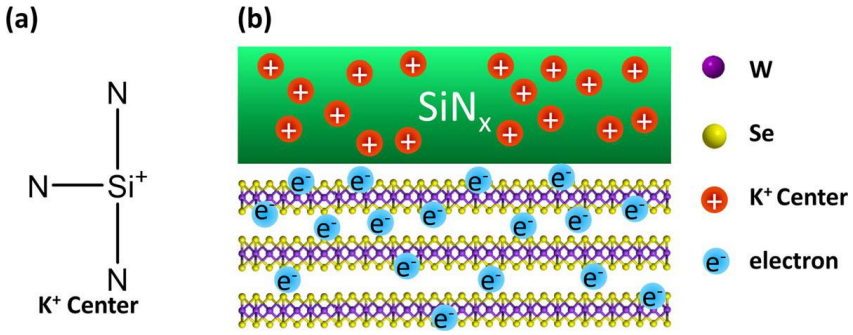

Figure 5.3 (a) The positively charged K^+ center found originating from $^+Si{\equiv}N_3$ dangling bonds. (b) Schematic of the doping mechanism of the SiN_x, where K^+ centers attract electrons inside the WSe_2, thus inverting it.
Source: Chen K., et al., (2014). Air stable n-doping of WSe_2 by silicon nitride thin films with tunable fixed charge density, *APL Materials*, 2, 092504 - 092504-7.

The entire deposition process is carried out at a fixed power, temperature, pressure and time with values of 20 W, 150 °C, 900 mTorr and 2 min, respectively. The thickness of SiN_x after this process is ~50 nm. The electron doping effect depends on the NH_3/SiH_4 ratio used during SiN_x deposition. With increase in NH_3/SiH_4 ratio, the device becomes more n-doped with higher n-channel conductance. Here, the ratio NH_3/SiH_4 refers to the ratio of NH_3 to 10% SiH_4 in Ar gas mixture [19].

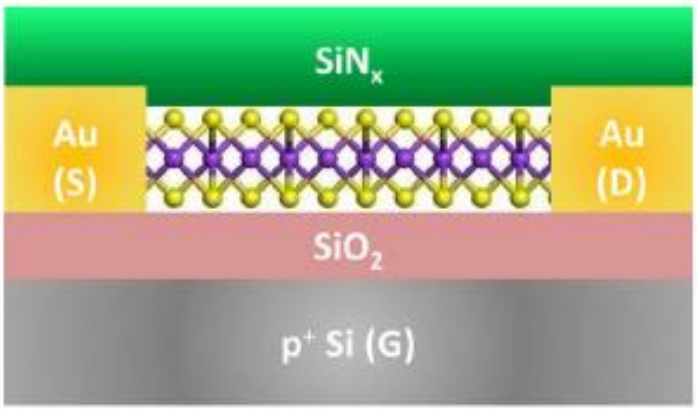

Figure 5.4 Schematic of the back gated WSe_2 device structure used to test the effect of NH_3/SiH_4 ratios during nitride deposition on doping.
Source: Chen K., et al., (2014). Air stable n-doping of WSe_2 by silicon nitride thin films with tunable fixed charge density, *APL Materials*, 2, 092504 - 092504-7.

CHAPTER 6

ELECTRICAL AND ELECTRONIC PROPERTIES OF WSe_2 ON DIFFERENT METAL FILMS

6.1 Resistivity

The resistivity of a material is the measure of the resistance a specific material offers to electrical conduction. Though all the materials resist the flow of electrical current, resistivity gives a figure for comparing which material allows or resists current flow. The electrical resistivity is the electrical resistance per unit length and per unit of cross-sectional area at a specified temperature. The SI unit of electrical resistivity is ohm·meter (Ω·m). It is commonly represented by the Greek letter ρ, rho. The equation used for electrical resistivity is:

$$\rho = R\frac{A}{l} \tag{6.1}$$

where, R is the electrical resistance of the material measured in ohms, l is the length of the piece of material used in meters, and A is the cross sectional area of the specimen measured in square meters.

All metals have resistivity in the region of ~ $10^{-8}\Omega\cdot m$ whereas, semiconductors have variable resistivity which strongly depends on the presence of impurities. Table 6.1 depicts some metals and their resistivity values measured at 295K.

Table 6.1 Electrical Resistivity at 295K

Conducting Material	Resistivity (Ω·m)
Silver	1.61×10^{-8}
Tungsten	5.3×10^{-8}
Aluminum	2.74×10^{-8}
Copper	1.68×10^{-8}
Iron	9.80×10^{-8}
Indium	8.75×10^{-8}
Gallium	14.85×10^{-8}
Platinum	10.40×10^{-8}
Lead	10.50×10^{-8}
Gold	2.20×10^{-8}

Source: http://hyperphysics.phy-astr.gsu.edu/hbase/Tables/rstiv.html

6.2 Work Function

The term - work function refers to the minimum energy required to remove an electron from the surface of a solid to vacuum. The work function is not a characteristic of a bulk material, but is a property of the surface of the material. The work function (W) for a given surface is represented as below:

$$W = -e\phi - E_F \tag{6.2}$$

In Equation 6.2, -e is the charge of an electron, ϕ is the electrostatic potential in vacuum (nearby to the surface) and E_F is the Fermi level inside the material. Table 6.2 shows values of work function in eV for some metals.

Table 6.2 Work Function of Some Metals

Metal	Work function (eV)
Selenium	5.11
Aluminum	4.08
Lead	4.14
Gold	5.1
Mercury	4.5

Source: https://public.wsu.edu/~pchemlab/documents/Work-functionvalues.pdf

6.3 Ohmic and Schottky Contacts

Metal-semiconductor contacts are required for any semiconductor device. There are basically two types of contacts- Ohmic contact and Schottky (rectifying) contact. A metal-semiconductor junction results in an Ohmic contact when the Schottky barrier height, ϕ_B, is zero or negative. Primarily, the charge carriers are free to flow in or out of the semiconductor providing least resistance across the contact. For an n-type semiconductor, for the Ohmic contact to take place, the work function of the metal must be close to or smaller than the electron affinity of the semiconductor. While considering p-type, the work function must be close to or larger than the sum of electron affinity and band gap energy. Typically, the work function of most metals is less than 5V and the electron affinity is around 4V; so it is troublesome to find a metal that provides Ohmic contact to p-type semiconductors.

On the other hand, Schottky contacts have a positive barrier at the interface. As doping is high in the semiconductor, the barrier separating metal from semiconductor is too thin. The width of such depletion region at the interface is of the order of 3nm or less, thus allowing carriers to pass through it easily. The doping density required for Schottky contacts is $10^{19}\,cm^{-3}$ or higher [23].

6.4 Energy Band Diagram for Metal-semiconductor Contacts

The barrier that is formed between metal and semiconductor can be recognized on an energy band diagram. To get the energy band diagram for a metal-semiconductor contact, consider the energy band diagram for metal and semiconductor individually. Figure 6.1 shows the energy band diagram for metal and semiconductor before contact is made.

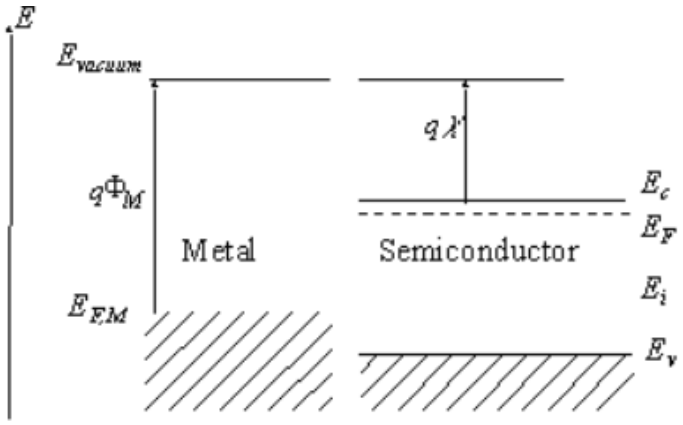

Figure 6.1 Energy band diagram of the metal and the semiconductor before contact.
Source: https://ecee.colorado.edu/~bart/book/book/chapter3/ch3_2.htm

Figure 6.2 shows the energy band diagram for a metal-semiconductor contact. The barrier height in this case, ϕ_B, is the potential difference between the Fermi energy of the metal and the band edge where majority charge carriers belong. From Figure 6.2 one can find that, for an n-type semiconductor, the barrier height is expressed as:

$$\phi_B = \phi_M - \chi \tag{6.3}$$

where, ϕ_M is the work function for a metal and χ is the electron affinity.

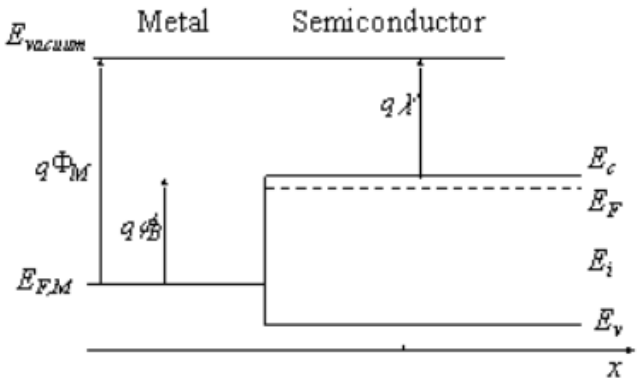

Figure 6.2 Energy band diagram for metal-semiconductor contact.
Source: https://ecee.colorado.edu/~bart/book/book/chapter3/ch3_2.htm

The barrier height for p-type semiconductor is given by the difference between the valence band edge and the Fermi energy in the metal, expressed as in Equation 6.4;

$$\phi_B = \frac{E_g}{q} + \chi - \phi_M \qquad (6.4)$$

Therefore, if the Fermi energy of the metal, as shown in Figure 6.2, is somewhere between the conduction and the valence band edge, then there will be a barrier formed for electrons and holes to pass by the metal-semiconductor junction.

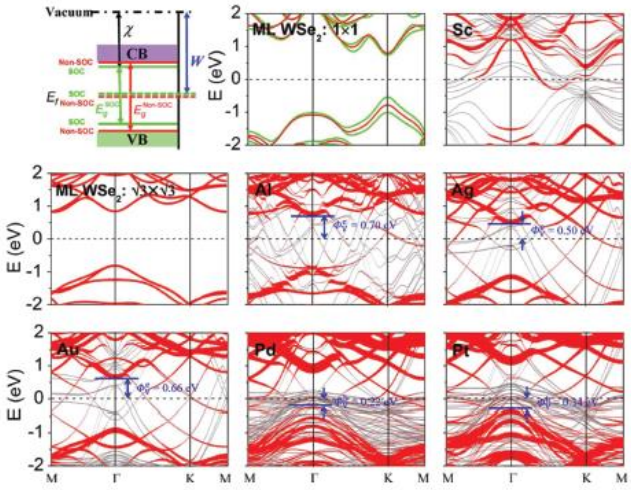

Figure 6.3 First panel: schematic illustration of the absolute band positions with respect to the vacuum level by the DFT method with and without inclusion of the spin orbital coupling (SOC) effects for ML WSe_2. The remaining: band structures of ML WSe_2 and ML WSe_2–Sc, –Al, –Ag, –Au, –Pt, and –Pt contacts, respectively. Gray line: metal surface bands; red line: bands of WSe_2 without considering the SOC effects. Green line: bands of WSe_2 with the SOC effects. The Fermi level is set at zero.

Source: Wang Y, et al., (2016). Does p-type ohmic contact exist in WSe_2-metal interfaces?, *Nanoscale*, 8, 1179-1191.

Figure 6.3 shows the band structure of monolayer (ML) WSe_2 and the combined systems. The band gap of ML WSe_2 becomes 1.57, 1.62, 1.56, 1.15 and1.51 eV in the ML WSe_2–Al, –Ag, –Au, –Pd and –Pt contacts, respectively, which are generally smaller than that (1.60 eV) of the pristine WSe_2 because of the

broadening of the energy bands induced by the perturbation of metal electrodes [3]. In ML WSe_2 -Al, -Ag and -Au contacts, the vertical Schottky barriers are n-type, while in ML WSe_2 -Pd and -Pt contacts, the vertical Schottky barriers are p-type.

6.5 Interface Modeling and Stability

A device often needs a contact with metal electrodes, and the formation of low-resistance metal contacts is a challenging task as it conceals the actual basic electronic properties of 2-D transition metal dichalcogenides. In this chapter, some electrical and electronic properties of 2-D tungsten diselenide devices, when kept in contact with different metal films, is illustrated. In addition to it, a comparative study is also presented regarding the interfacial properties between monolayer/bilayer (ML/BL) WSe_2 with respect to different metal contacts such as Sc, Al, Ag, In, and Pt.

According to some tests done earlier, six layers of metal atoms with different orientations are used to model the metal surface, as six layer metal atoms can have varied properties. As studied by Wang Y. et al. regarding the metal atoms, Sc has (0001) orientation and Al, Ag, Au, Pt and Pd has (111) orientation [3]. The most stable configurations of the monolayer WSe_2-metal interfaces is shown in Fig. 6.4.

As shown in Fig. 6.4(c), on the Sc(0001) surface, the W atoms in the primitive cell reside above the top metal atoms, and the Se atoms are above the second layer metal atoms. From Fig. 6.4(d), the W atoms in the supercell for the Al and Pt (111) surfaces are above the centers of the triangles formed by the fcc, hcp, and top sites, while the three pairs of Se atoms reside above the fcc, hcp, and top sites respectively. In a similar pattern, we get the stable configurations for other metal atoms. The most stable configurations of the BL WSe_2-metal interfaces are similar to corresponding ones for the MLWSe_2-metal interfaces.

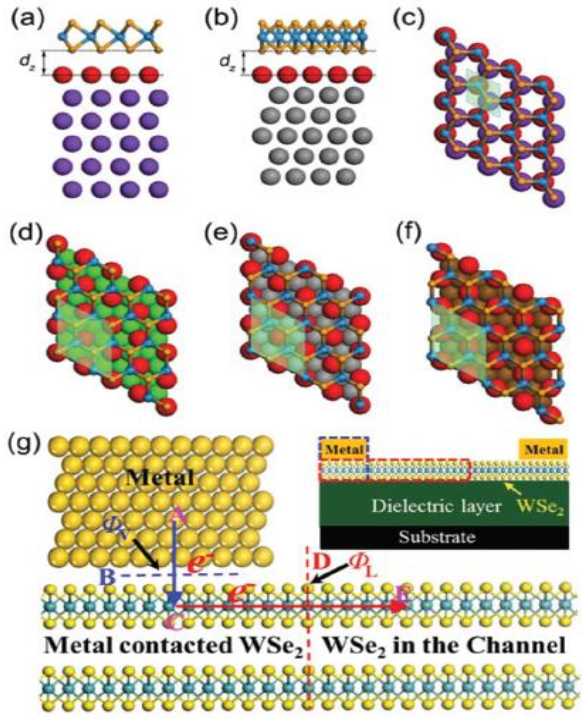

Figure 6.4 Interfacial structures of the most stable configuration for MLWSe$_2$on metal surfaces. Side views of (a) WSe$_2$ on the Sc(0001) surface and (b) on other metal surfaces. Top views of contacts (c) Sc–WSe$_2$, (d)Al/Pt–WSe$_2$, (e) Pd–WSe$_2$, (f) Ag/Au–WSe$_2$. d_z is the equilibrium distance between the metal surface and the bottom layer WSe$_2$. The rhombi plotted in light green shadow shows the unit cell for each structure. (g)Schematic cross-sectional view of a typical metal contact to intrinsicWSe$_2$. A, C, and E denote the three regions while B and D are the two interfaces separating them. Blue and red arrows show the pathway (A →B → C → D → E) of electron injection from the contact metal (A) to theWSe$_2$ channel (E). Inset figure shows the typical topology of a WSe$_2$ field effect transistor.
Source: Wang Y., et al., (2016). Does p-type ohmic contact exist in WSe$_2$-metal interfaces?, *Nanoscale*, 8, 1179-1191.

The binding energy per interfacial W atom is defined as

$$E_b = (E_{WSe2} + E_{metal} - E_{WSe2\text{-}metal})/ N_W \qquad (6.5)$$

where E_{WSe2} is the relaxed energy for the WSe$_2$, E_{metal} is the relaxed energy for the metal surface and $E_{WSe2\text{-}metal}$ for the combined system per supercell, and N_W is the number of interface W atoms per supercell. E_b values range from 0.160 to 1.049 eV as listed in Table 6.3.

Table 6.3 Calculated Interfacial Properties of ML and BL WSe_2 on the Metal Surfaces.

			ML WSe_2				Reference
Metal	a_{hex}^{cexc} (Å)	**W_M (eV)**	**d_z (Å)**	**E_b (eV)**	**W (eV)**	**SBH (eV)**	
Sc	3.308	3.60	2.736	0.918	3.75	0.29[b](0.25[b])[d]	[3]
Al	5.720	4.12	2.959	0.288	4.15	0.70[b]	[3]
Ag	5.778	4.49	2.693	0.302	4.26	0.50[b]	[3]
Au	5.768	5.23	2.712	0.182	4.71	0.66[b](0.70[b])[a]	[3]
Pd	5.500	5.36	2.395	0.602	4.84	0.22[c](0.35[c])[a](0.23[c])[d]	[3]
Pt	5.549	5.76	2.652	0.525	5.22	0.34[c](0.34[c])[e](0.00[c])[d]	[3]
			BL WSe_2				
Metal	a_{hex}^{cexc} **(A°)**	**W_M (eV)**	**d_z (A°)**	**E_b (eV)**	**W (eV)**	**SBH (eV)**	
Sc	3.308	3.60	2.512	1.049	3.94	0.16[b] (0.25[b])[d]	[3]
Al	5.720	4.12	2.885	0.367	4.16	0.37[b]	[3]
Ag	5.778	4.49	2.684	0.240	4.56	0.30[b]	[3]
Au	5.768	5.23	2.773	0.160	4.85	0.58[c]	[3]
Pd	5.500	5.36	2.271	0.706	5.05	0.27[c] (0.09[c])[d]	[3]
Pt	5.549	5.76	2.770	0.597	5.21	0.32[c] (0.00[c])[d]	[3]

In Table 6.3, a_{hex}^{cexc} represents the experimental cell parameters of the surface unit cell shown in Fig. 6.3 for various metals given above. The equilibrium distance d_z is the averaged distance between the surface Se atoms of WSe_2 and the relaxed position of the topmost metal layer in the z direction. E_b is the binding energy per surface W atom between WSe_2 and a given metal. W_M and W are the calculated work function values for the clean metal surface and WSe_2-metal contact, respectively. The SBHs are obtained by the band calculation with inclusion of the Spin-Orbit Coupling (SOC). Electron SBH is given for the n-type Schottky barrier and hole SBH is given for the p-type Schottky barrier. The Schottky barrier is always formed at the vertical direction except for the Sc surface.

6.6 Schottky Barrier Height

The ML WSe_2 has a band gap of 1.60 eV when the SOC is absent. The valence and conduction band of ML WSe_2 are strongly destroyed when getting in contact with Sc, which results in an absence of its vertical Schottky barrier. As there is weak interaction for the WSe_2 and Al, Ag and Au surfaces, we can identify the band structures for those interactions. Vertical Schottky barrier $\Phi_V^{e/h}$ for these weak or medium bonding (Fig. 6.4(g)) is obtained by the energy difference between E_f of the interfacial system and the CBM or VBM of the contacted WSe_2. In ML WSe_2 -Al,-Ag and -Au contacts, the vertical Schottky barriers are n-type with electron SBH of Φ_V^e = 0.70, 0.50 and 0.66 eV, respectively. In ML WSe_2-Pd and -Pt contacts, the vertical Schottky barriers are p-type with hole SBH of Φ_V^h = 0.22 and 0.34 eV, respectively [3]. The schematic illustration of the band positions is described in detail in Section 6.4.

The zero bias barrier height ϕ_{bo} and flat band barrier height ϕ_{bf} are calculated using the following equations [8]:

$$\phi_{bo} = \frac{kT}{q} \ln\left(\frac{AA^*T^2}{N_A}\right) \tag{6.6}$$

$$\phi_{bf} = n\phi_{bo} - (n-1)\frac{kT}{q} \ln\left(\frac{N_V}{N_A}\right) \tag{6.7}$$

6.7 Photovoltage for WSe_2 Schottky barriers

Photovoltage is measured at the Schottky barriers of Cu, In and Au with selenium grown p-WSe_2 single crystals. In Figure 6.2(a), the coverage dependence of source-induced photovoltages for Schottky barriers that are prepared at T = 85K substrate temperature is shown. The smaller initial value for the Au/p -WSe_2 junction is due to

the low barrier height of $\Phi_{B,Au}$ = 0.76 eV [5], though all other samples also show the same behavior. The thick solid line in the figure corresponds to a calculated value of surface photovoltage using shunt resistances as indicated in the upper scale. The shunt resistance R_{sh} influences the photovoltage via the current-voltage relation given by:

$$J = J_{ph} - J_o \times (e^{qv/kT} - 1) + \frac{V}{R_{sh}} \qquad (6.8)$$

here, J is the total current density, J_{ph} is the photocurrent density which is induced by the excitation source ($J_{ph} \sim 10^{-3}$ mA/cm^2 [5]), J_o is the dark saturation current density of the junction, and V is the voltage. Here, the researchers have used an effective Richardson constant for p-WSe_2 of 27.6 A/cm^2 K^2 for the calculations [5].

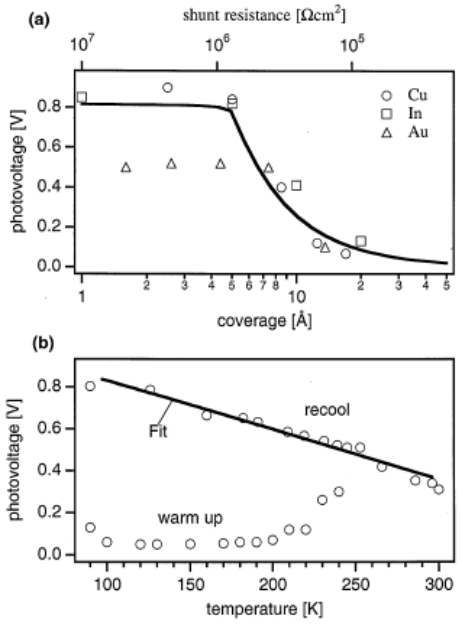

Figure 6.5 (a) Evolution of photovoltage from Schottky barriers formed between Cu, Au, In and p-WSe_2 at T ~ 85K. (b) Temperature dependence of photovoltage of In/p-WSe_2 Schottky barrier formed at T ~ 85K. The solid line corresponds to a least-squares fit of thermionic emission model of experimental points during recooling.
Source: A. Klein, et al., (1998). Photovoltaic properties of WSe_2 single-crystals studied by photoelectron spectroscopy, *Solar Energy Materials and Solar Cells*, 51, 181-191

At low temperatures, there is a decrease in photovoltages with increase in film thickness during the formation of Schottky barriers on III-V compound

semiconductors. The shunt resistance is introduced by the growing metal film which eventually reduces the lateral conductivity of the sample surface and on heating it further, the lateral conductivity of the sample surface drops down. After clustering of the metal film has occurred, In/p-WSe_2 interfaces shows ideal collection of photogenerated charge carriers. This is also understood from Fig. 6.5(b) where the synchrotron-induced surface photovoltage is shown during the temperature cycle. Comparable results are also observed for Cu/p-WSe_2 and Au/p-WSe_2 interfaces [5].

6.8 I-V Characteristics

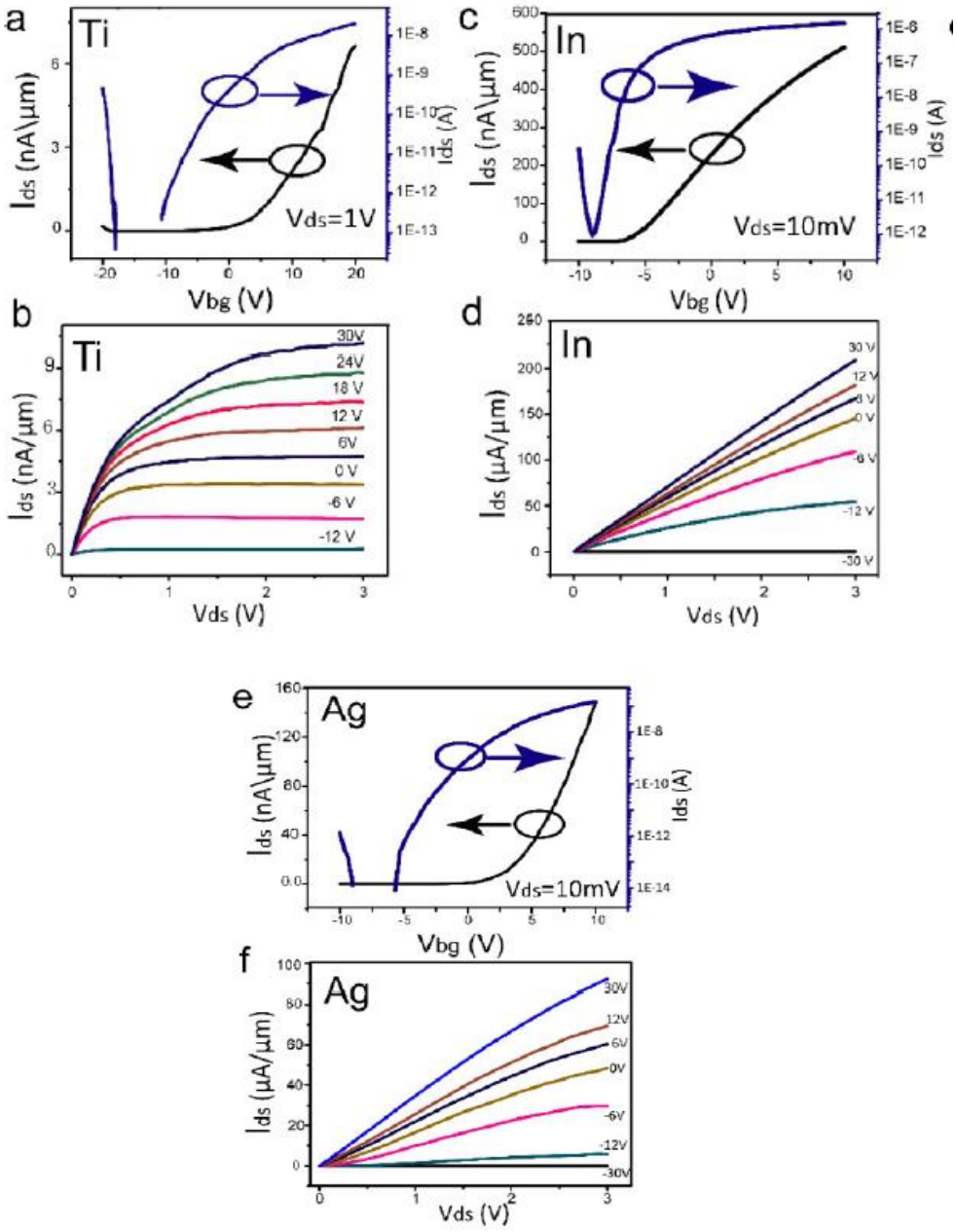

Figure 6.6 Transfer characteristics of back gated ML WSe_2 FETs with (a) Ti (10 nm)/Au (100 nm), (c) In (10nm)/Au(100nm),(e)Ag(10nm)/Au(100nm). (b,d,f) Corresponding I_{ds}-V_{ds} curve from device (a,c,e) respectively. Device sizes (length/width) are (a) 1μm/ 3μm, (c) 3.5μm/ 3μm and (e) 1.5μm/ 1μm.
Source: Liu W., et al., (2013). Role of Metal Contacts in Designing High-Performance Monolayer n-type WSe_2 Field Effect Transistors, *ACS Publications*, 13, 1983-1990

The general relationship between current and voltage for a Schottky barrier diode is expressed in Equation (6.9) as [1] :

$$I = I_0\left[exp\left(\frac{q(V-IR_s}{nkT}\right) - 1\right] \quad (6.9)$$

where, q is the electronic charge, V is the applied voltage across the diode, k is the Boltzmann's constant, T is the absolute temperature in K, n is the ideality factor, I_0 is the reverse saturation current and IR_s refers to the voltage drop across the junction.

Here, WSe_2 FET devices are fabricated with In, Ag and Ti. Figure 6.6(a, c, e) shows the transfer I-V curves of the back-gated WSe_2 FETs with Ti (10 nm)/Au (100 nm), In (10nm)/Au(100nm), and Ag(10nm)/Au(100nm) contacts. The contacts for all the three metal-contacts is ohmic. At high negative voltage, small hole currents (3-5 orders lower than electron current) are observed in ML WSe_2. The field effect mobility of WSe_2 FET with Ti contact is in the range of0.01 - 2 $cm^2/V{\cdot}s$ [17]. But, for In and Ag contacts which has low contact resistance, they have improved current drives as shown in Figure 6.6(c, e). As shown in Figure 6.6(d) for the In-WSe_2 device, the ON- current is around 210µA/µm for V_{bg} = 30V and V_{ds} = 3V. However, the ON current does not saturate at these voltage values, which indicates that higher ON currents are also possible. This high ON current corresponds to a current density of 3.25×10^7 A/cm^2, which is about 50 to 60 times larger than the maximum current density of copper interconnects involved in nanoscale ICs and only about an order of magnitude below that of graphene [17]. The I_{ds}-V_{ds} curve for the same In-WSe_2 FET shows a linear behaviour as in Figure 6.6(d), which indicates that this metal-semiconductor contact is ohmic in nature. In addition to indium's low contact resistance behavior, it has poor adhesion with the substrate and also low melting point of 156°C which limits its usage as a contact metal.

In the case of Ag-WSe_2 FET device, as shown in Figure 6.6(e, f), the transfer output- curve has linear behavior indicating Ag to form ohmic contact with WSe_2. The mobility of this device is in the range of 16-44 $cm^2/V{\cdot}s$, which is comparatively higher than that of Ti-WSe_2 FET devices. The ON current for Ag-WSe_2 is 2 to 4 times lower than that of the In-WSe_2 FET. The reason for low ON current is the high

contact resistance of Ag with WSe_2. The ON/OFF ratio for this device is greater than 10^8 [17]. Further, in the case of Ti metal-contact, The I_{ds}-V_{ds} curve shows very high current saturation (which is not observed for In, while there is slight saturation for Ag contact). This phenomenon indicates that the current saturation of ML WSe_2 FET device is possibly influenced by the contact metal. Also it can be observed from the figure that the modulation in threshold voltage (V_t) is influenced by the contact-metal. From Figure 6.6(c), the V_t for the case of In metal is extracted to be -7V [4]. Because of this negative voltage, V_{gs_eff} - V_t is greater than V_{ds_eff} and thus the device operates in the linear region. The statement stated above explains the reason why we observe the absence of saturation current in the case of In contact.

6.9 Metal-Semiconductor Junction Capacitance

We can obtain the capacitance as a function of the applied voltage by taking the derivation of the charge with respect to the applied voltage, which gives:

$$C_j = \left|\frac{dQ_d}{dV_a}\right| = \sqrt{\frac{q\varepsilon_s N_d}{2(\phi_1 - V_a)}} = \frac{\varepsilon_s}{x_d} \tag{6.10}$$

The last term in Equation (6.10) explains that the charge added or removed from the depletion layer takes place at the edge of the depletion region which depends on the increase or decrease in the applied voltage. The term also indicates that it is a parallel plane capacitor expression, but basically it is not because in the metal-semiconductor junction capacitance; the width x_d is variable and changes with the applied voltage [23].

CHAPTER 7

EXPERIMENTAL RESULTS FROM LITERATURE AND ANALYSIS

7.1 Case Study 1: WSe_2-Indium Metal Contact

(a) Experimental Results

Mathai A., et al, in their paper, carried out a schematic investigation on the temperature dependence of the electrical properties of 1000 Å metal thickness In-pWSe_2 diode. In this investigation, p type WSe_2 crystals with $10^{16}/cm^3$ acceptor density were grown by direct vapor transport technique and the carrier concentration of the grown crystals were determined by Hall effect technique. The indium metal used for the investigation is of high purity (Aldrich 99.99%) which was thermally evaporated at the rate of 0.2 Å/s onto the front cleaved surface of the crystal to form circular Schottky contacts of area of 3.6×10^{-3} cm^2. The pressure inside the chamber was $\approx 10^{-6}$ Torr [1]. To form the back ohmic contact, silver paste was brushed on the uncleaved side of the crystal.

To characterize the current-voltage-temperature relationship, measurements were carried out in the temperature range of 140-300K using Keithley 2400 Sourcemeter and Lakeshore Closed Cycle Refrigerator at an interval of 20K. Figure 7.1 shows the I-V curve of In-pWSe_2 diode at 1000Å metal thickness.

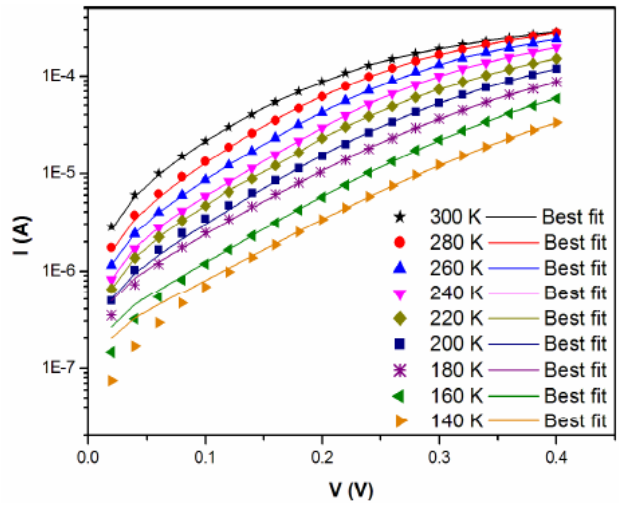

Figure 7.1 Experimental and simulated I-V curve of In-pWSe_2 (1000 Å) Schottky diode at different temperatures.
Source: Bobby A., et al, (2011). Schottky Barriers on Layered Anisotropic Semiconductor- WSe_2 -with 1000 Å Indium Metal Thickness, *Materials Sciences and Applications*, 2, 1000-1006.

(b) Analysis

Based on this experimental investigation of current-voltage characteristics at different temperature range for indium metal on WSe_2,Figures7.2to 7.9are drawn. The data were analyzed using the WebPlot Digitizer. The graph is represented separately for different temperatures. In the graph, the blue lines show the plots of the observed values while the black line is the linear line which gives the best fit.

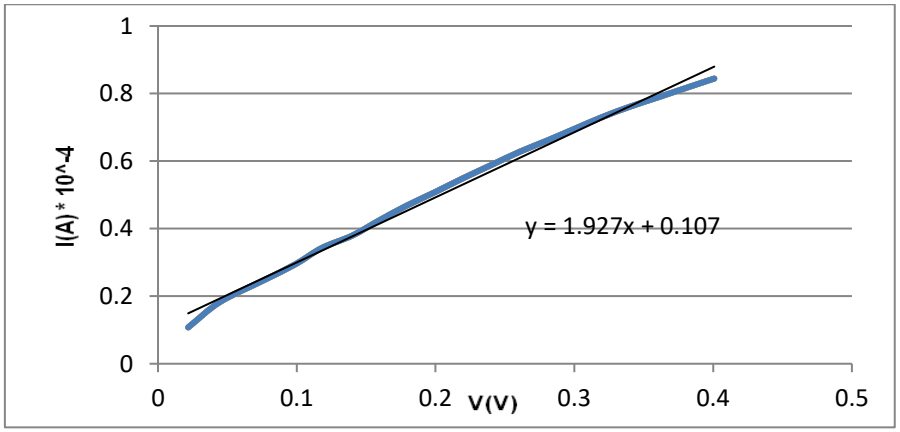

Figure 7.2I-V curve at 140K for In-pWSe_2.

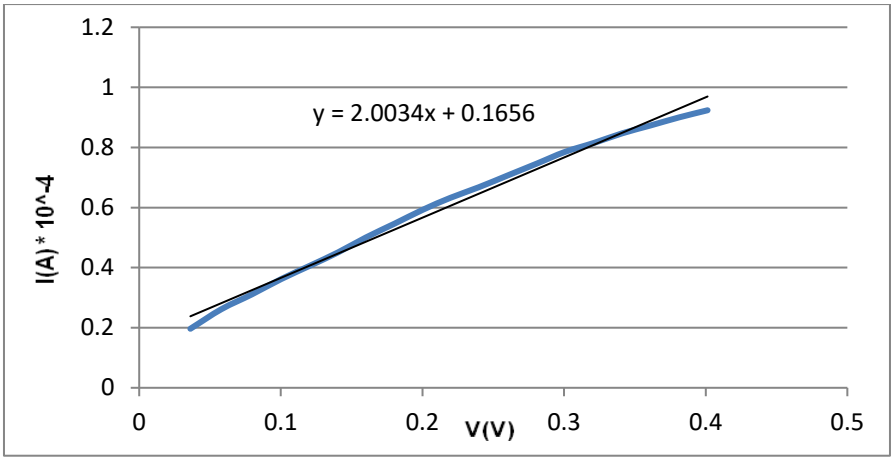

Figure 7.3 I-V curve at 160K for In-pWSe$_2$.

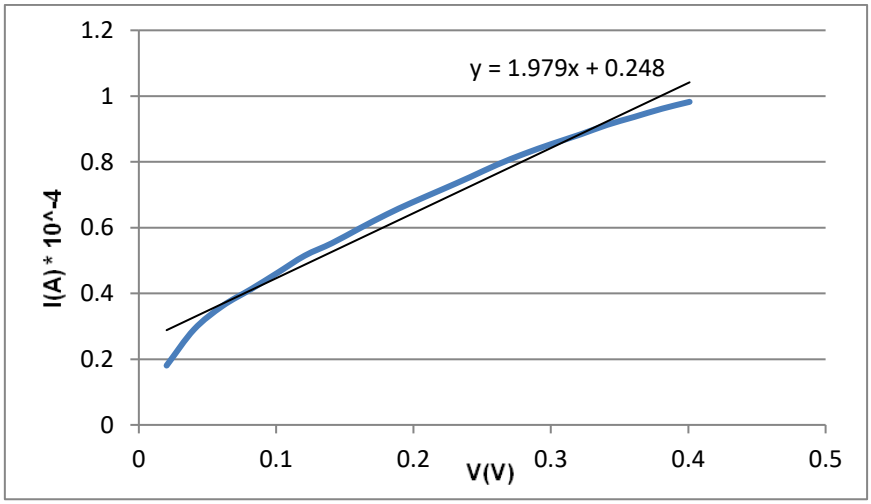

Figure 7.4 I-V curve at 180K for In-pWSe$_2$.

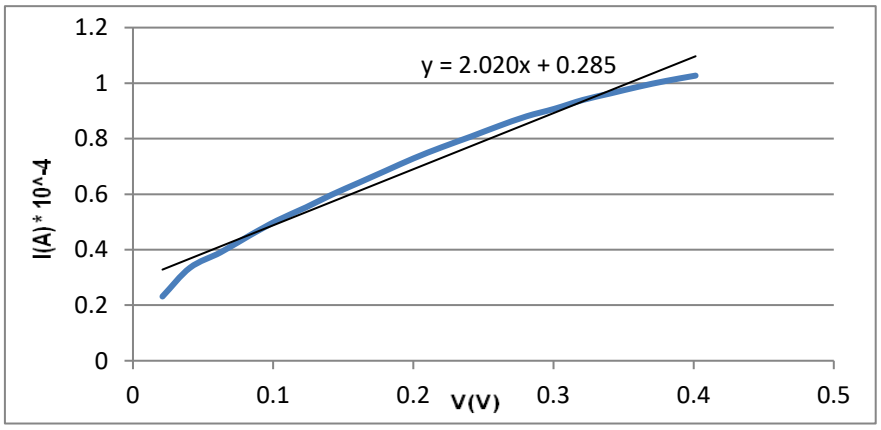

Figure 7.5 I-V curve at 200K for In-pWSe$_2$.

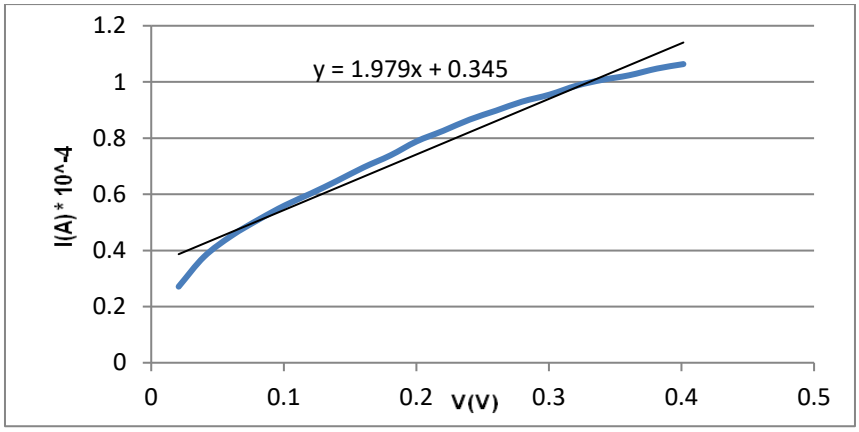

Figure 7.6 I-V curve at 220K for In-pWSe$_2$.

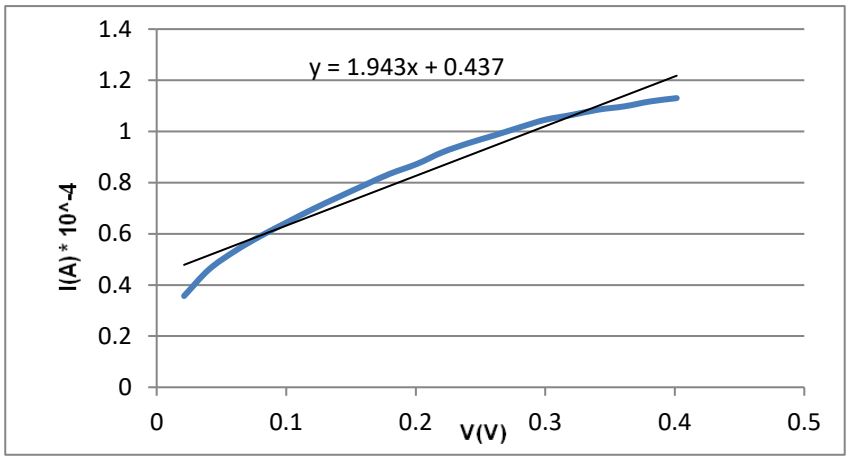

Figure 7.7 I-V curve at 260K for In-pWSe$_2$.

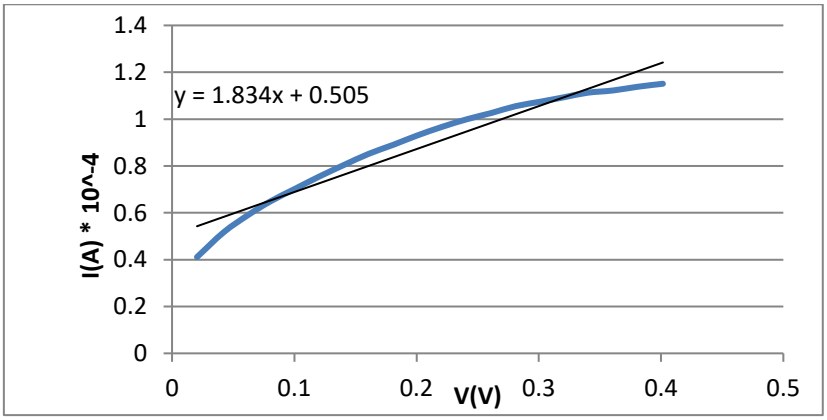

Figure 7.8 I-V curves at 280K for In-pWSe$_2$.

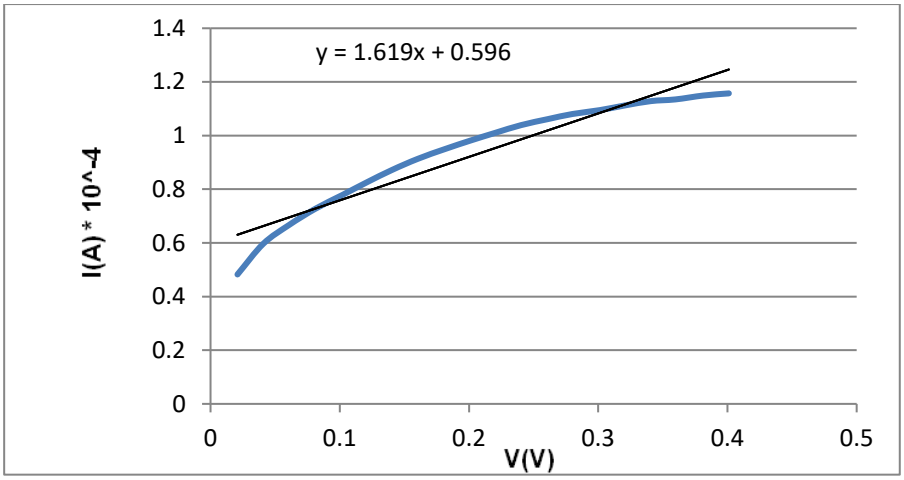

Figure 7.9 I-V curves at 300K for In-pWSe_2.

Table 7.1 Temperature Dependence of Slope for WSe_2-In Metal Contact

Metal-Semiconductor contact	**Temperature (K)**							
WSe_2-In	140	160	180	200	220	260	280	300
Slope	1.927×10^{-4}	2.003×10^{-4}	1.979×10^{-4}	2.020×10^{-4}	1.979×10^{-4}	1.943×10^{-4}	1.834×10^{-4}	1.619×10^{-4}

From Table 7.1, it is generally observed that, with increase in temperature, the value of slope decreases. But, we observe some discrepancy at points below 200 K, even though good linear fit is obtained in the high temperature range. These discrepancies imply that the current transport is not purely thermionic but has multiple charge conduction mechanisms in the low temperature regime.

To avoid this irregularity, we can consider a combined effect model, consisting of thermionic emission current, and currents due to tunneling and generation-recombination which is expressed as:

$$I=\left[I_o \exp\left(\frac{q(V-IR_s)}{n_{ap}kT}\right) + I_{oTN} \exp\left(\frac{(V-IR_s)}{E_0} - 1\right) + I_{oGR} \exp\left(\frac{q(V-IR_s)}{2kT}\right)\right]\times$$

$$\left[1 - \exp\left(\frac{-q(V-IR_s)}{kT}\right)\right] \qquad (7.1)$$

where, I_{0TN} and I_{0GR} are the tunneling and generation recombination saturation current respectively.

Using equation(7.1), the irregularity at low temperatures can be avoided. Table 7.2 shows the change in values for slope after considering the combined effect model. The mean barrier height ϕ_{bo} of WSe_2-In Schottky Barrier diode comes out to be 0.87 eV with a standard deviation of 0.128 eV [1].

Table 7.2 Temperature dependence of slope for WSe_2– In metal contact after combined model effect

Metal-Semiconductor contact	**Temperature (K)**							
WSe_2-In	140	160	180	200	220	260	280	300
Slope	2.03×10^{-4}	2.022×10^{-4}	2.013×10^{-4}	2.002×10^{-4}	1.979×10^{-4}	1.943×10^{-4}	1.834×10^{-4}	1.619×10^{-4}

Concluding from Table 7.2, the value of slope decreases constantly with increase in temperature and the irregularities observed at low temperature are removed after the combined effect model.

7.2 Case Study 2: WSe_2- Aluminum Metal Contact

(a) Experimental Results

In considering the aluminum contact on p type WSe_2 crystal, the researchers have aimed to investigate the current transport mechanisms of Al-pWSe_2 Schottky barrier diode for a wide range of temperatures from 140-300 K. For this investigation, the crystals of p-WSe_2 were grown by vapor transport technique with excess Se used in a sealed quartz tube. The vessel was heated for a week under constant temperature of 1333 K with appropriate temperature gradient. At the end, single crystals of WSe_2 were found in the vessel. The crystals formed had acceptor density of $10^{16}/cm^3$ and Hall effect technique was used for determining that they are p-type crystals. Pure aluminum (Aldrich 99.99%) was used to create the ohmic contacts on the surface of

the crystal by thermal evaporation process (the rate of evaporation was 0.2 Å) at a vacuum level of 1.33×10^{-7} Pa [8].

Figure 7.8 shows the data of current-voltage with varying temperature that was acquired by A.J. Mathai and K.D. Patel in their investigation. In the figure, the best fit I-V-T characteristics are shown for Al-pWSe_2 Schottky diode with 1000 Å Al thickness.

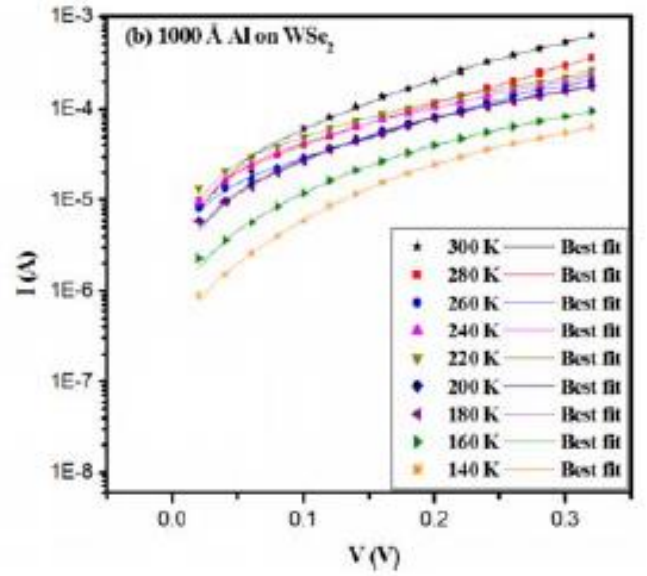

Figure 7.10 Experimental and simulated I-V curve of the prepared Al-pWSe_2 Schottky diodes at different temperatures.
Source: Mathai A., et al, (2010). Schottky diode characteristics: Aluminum with 500 and 1000 Å thicknesses on p type WSe_2 crystal, *Wiley-VCH*, 7, 717-724.

(b) Analysis

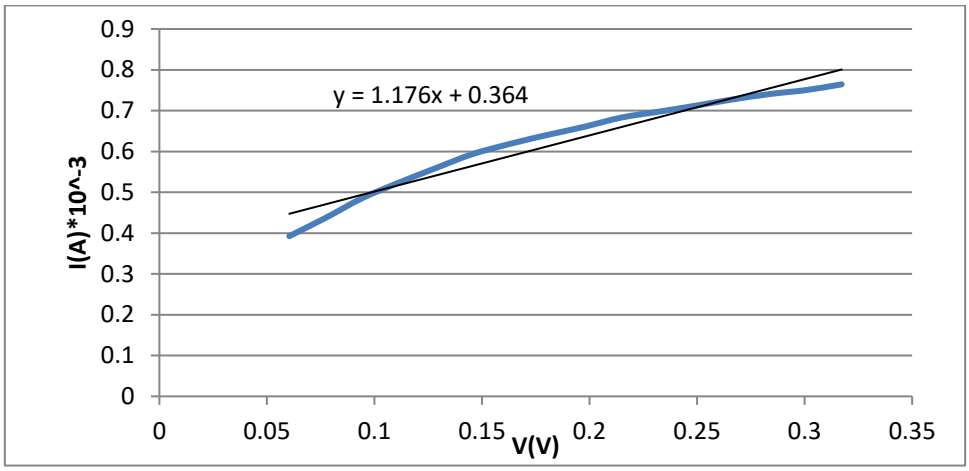

Figure 7.11 I-V curve at 140K for Al-pWSe$_2$.

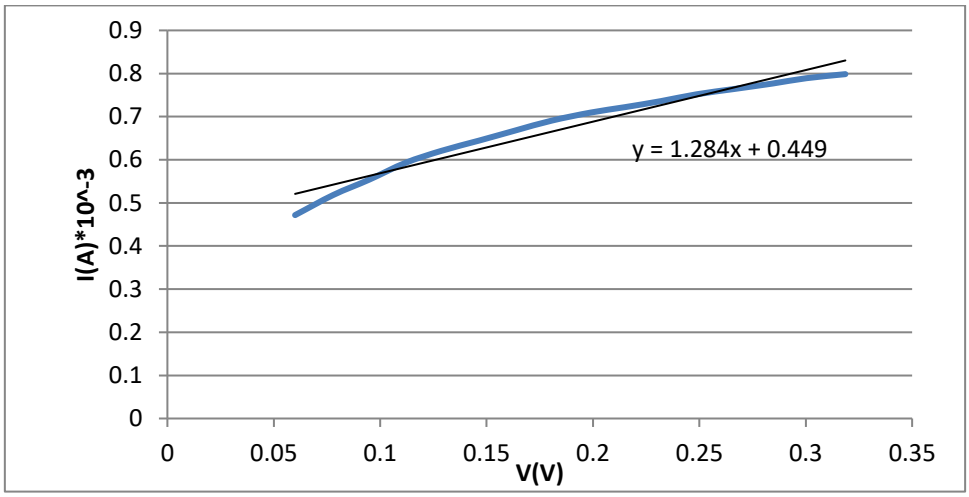

Figure 7.12 I-V curve at 160K for Al-pWSe$_2$.

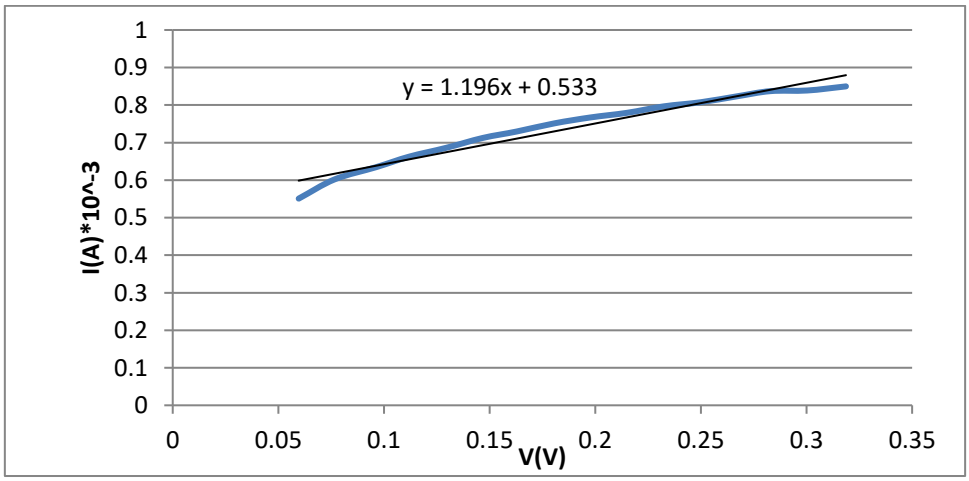

Figure 7.13 I-V curve at 200K for Al-pWSe$_2$.

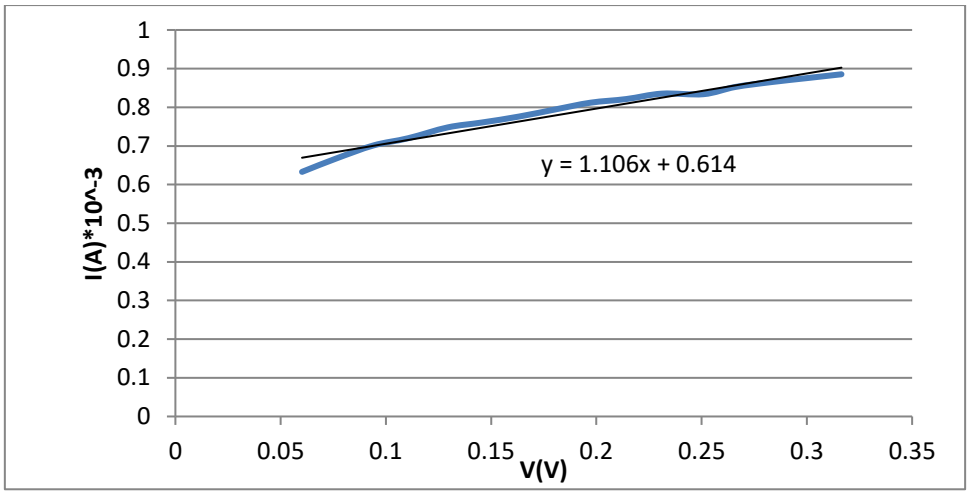

Figure 7.14 I-V curve at 220K for Al-pWSe$_2$.

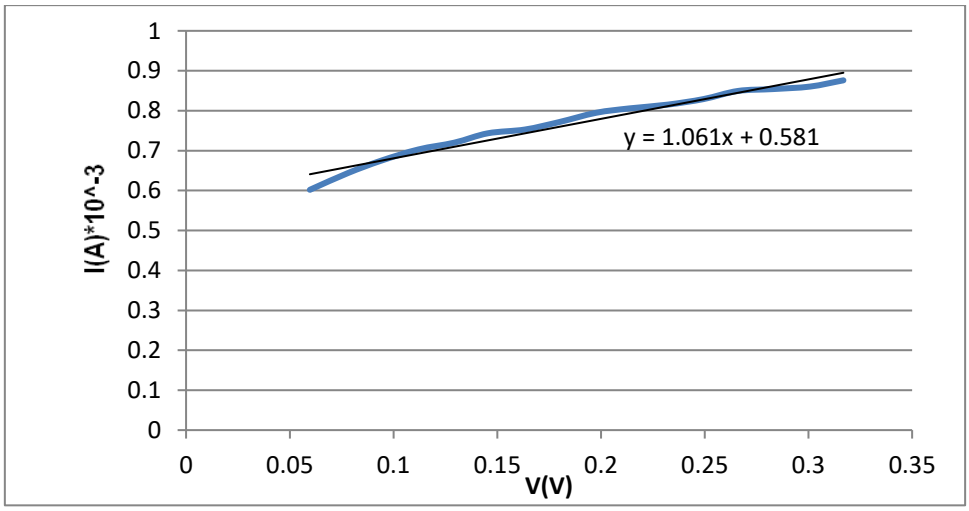

Figure 7.15 I-V curve at 240K for Al-pWSe$_2$.

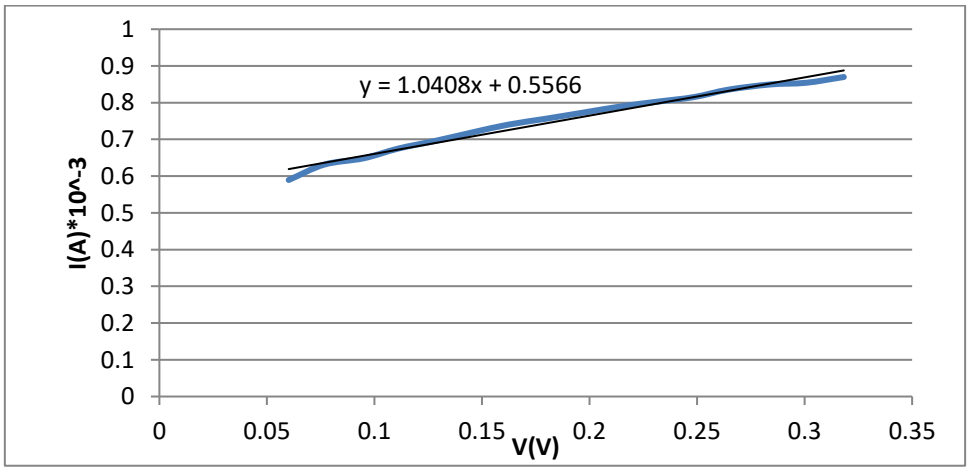

Figure 7.16 I-V curve at 260K for Al-pWSe$_2$.

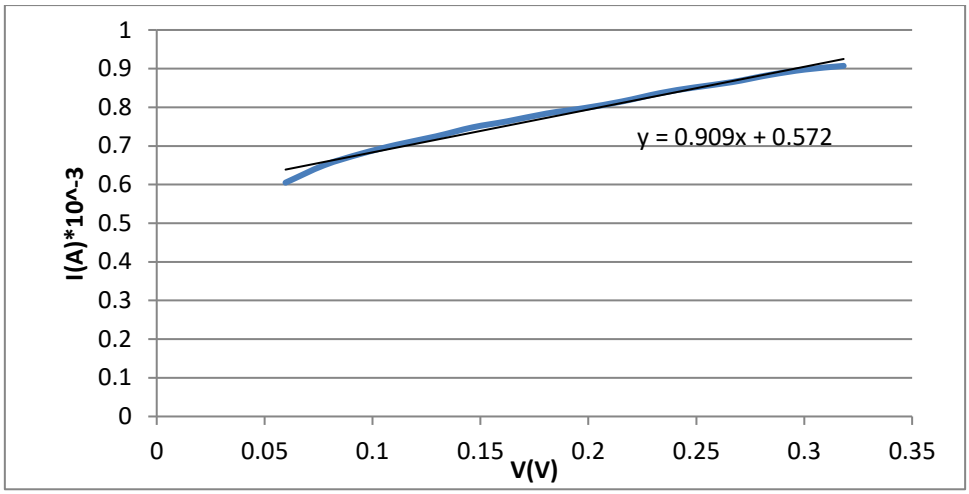

Figure 7.17 I-V curve at 280K for Al-pWSe_2.

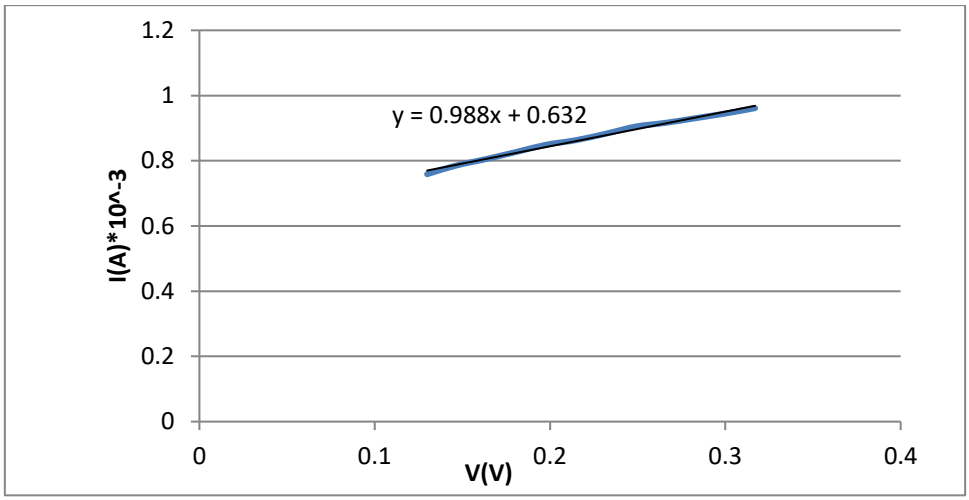

Figure 7.18 I-V curve at 300K for Al-pWSe_2.

Table 7.3 Temperature Dependence of Slope for WSe_2-Al Metal Contact

Metal-Semiconductor contact	**Temperature (K)**							
WSe_2-Al	140	160	200	220	240	260	280	300
Slope	1.176×10^{-3}	1.284×10^{-3}	1.196×10^{-3}	1.106×10^{-3}	1.061×10^{-3}	1.040×10^{-3}	0.909×10^{-3}	0.988×10^{-3}

The analysis and observation done in this case is similar to the analysis performed for WSe_2-In Schottky Barrier diode in case study 1. The irregularity that we observe at low temperatures, in which the slope value is not discrete with increase

in temperature is due to the multiple charge transport mechanisms. The problem can be resolved by using Equation (7.1). The mean zero bias barrier height ϕ_{bo} is 0.88 eV for WSe_2-Al Schottky Barrier diode [8].

Table 7.4 Temperature Dependence of Slope for WSe_2– Al Metal Contact after combined model effect

Metal-Semiconductor contact	**Temperature (K)**							
WSe_2-Al	140	160	200	220	240	260	280	300
Slope	1.376×10^{-3}	1.193×10^{-3}	1.196×10^{-3}	1.084×10^{-3}	1.061×10^{-3}	1.040×10^{-3}	0.909×10^{-3}	0.988×10^{-3}

Similar to Indium metal contact studied earlier, the results for WSe_2–Al, after considering the combined effect model, turned out to be the same. Thus, we can conclude that irrespective of the metal contact used, the value of slope decreases and the discrepancies are removed.

7.3 Case Study 3: Analysis of WSe_2 -Gallium Metal Contact

The Current-Voltage analysis of gallium metal contact on WSe_2 crystal was done in the temperature range of 80-400 K. Figures 7.19-7.26 represent the I-V curves at different temperatures for this system.

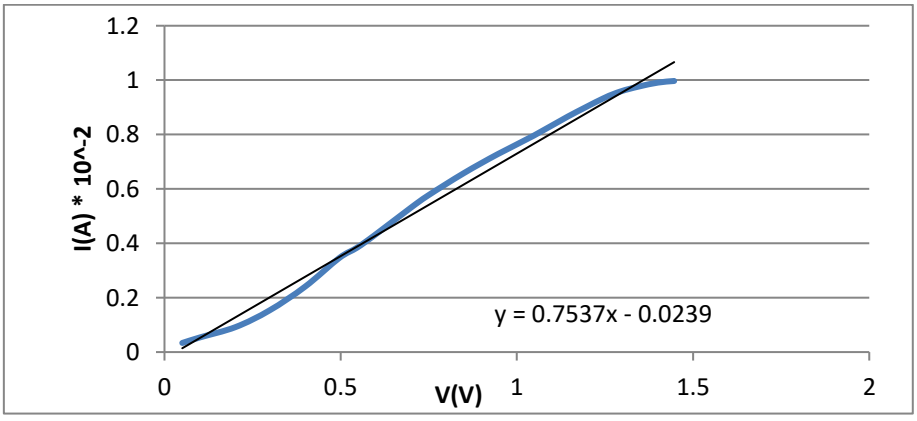

Figure 7.19 I-V curve at 80K for Ga-pWSe_2.

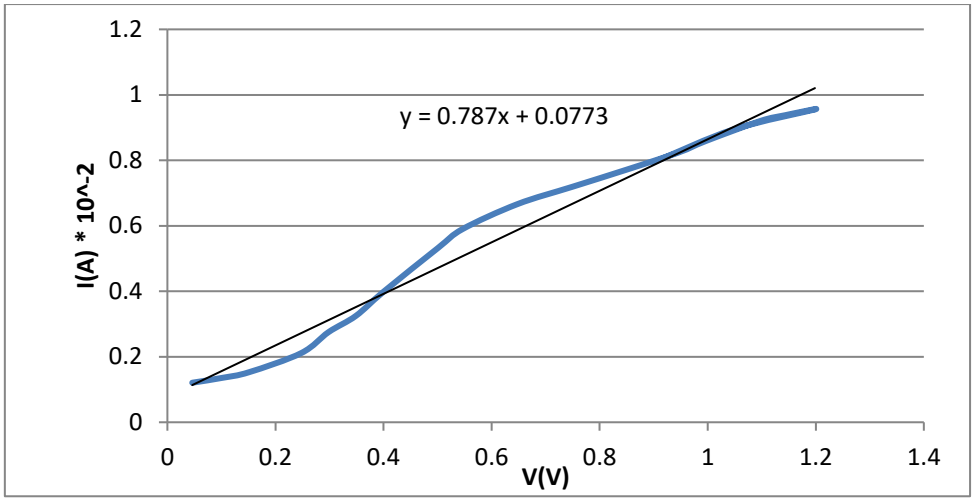

Figure 7.20 I-V curve at 170K for Ga-pWSe$_2$.

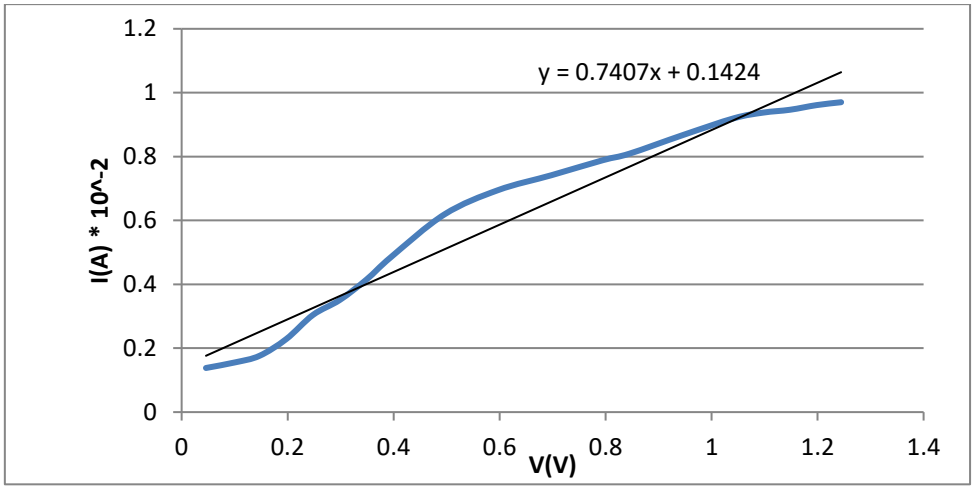

Figure 7.21 I-V curve at 200K for Ga-pWSe$_2$.

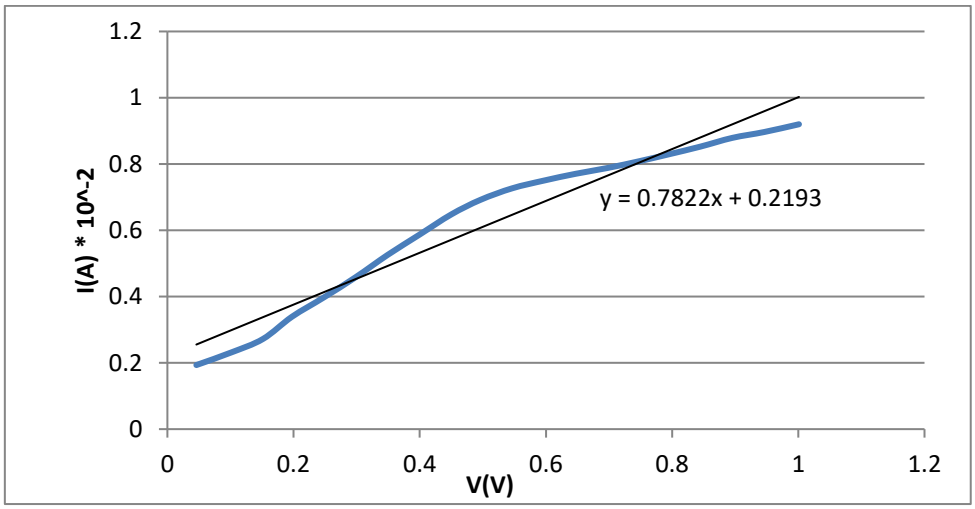

Figure 7.22 I-V curve at 230K for Ga-pWSe$_2$.

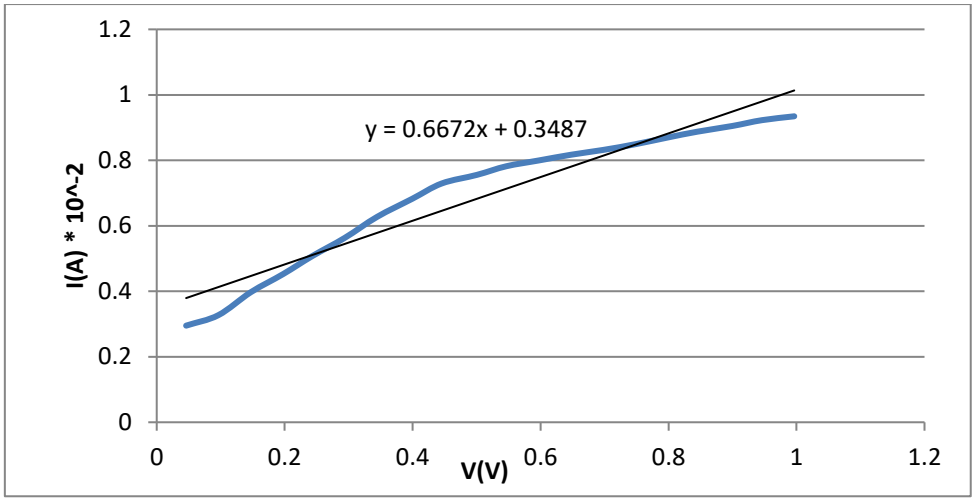

Figure 7.23 I-V curve at 260K for Ga-pWSe$_2$.

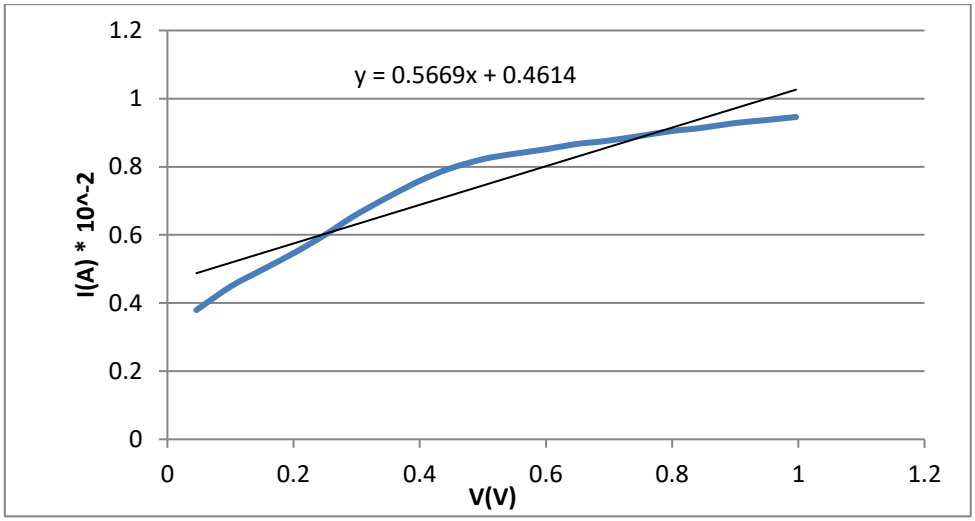

Figure 7.24 I-V curve at 290K for Ga-pWSe$_2$.

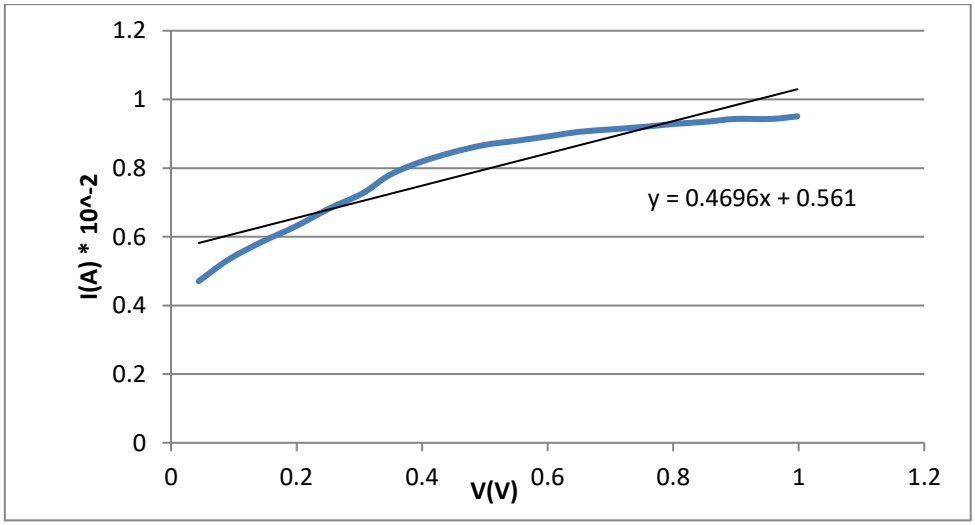

Figure 7.25 I-V curve at 320K for Ga-pWSe$_2$.

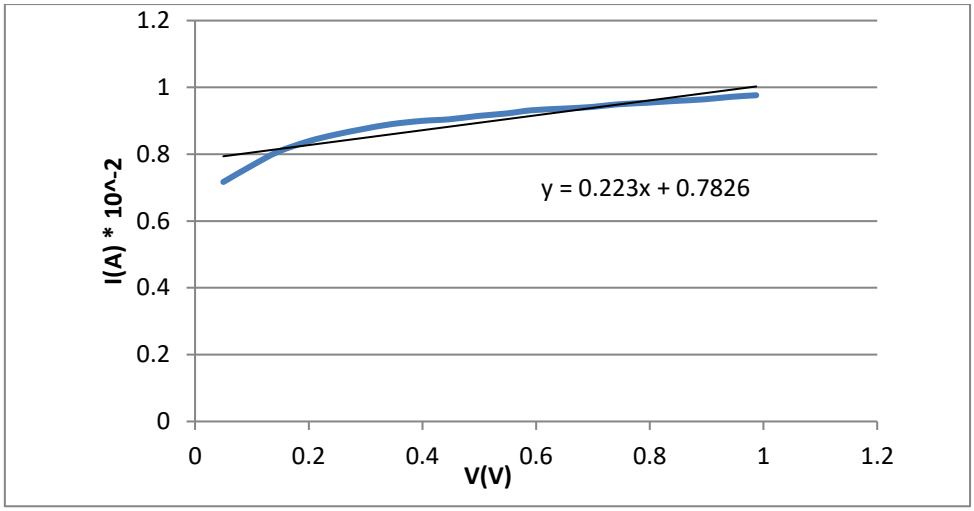

Figure 7.26 I-V curve at 400K for Ga-pWSe_2.

Table 7.5 Temperature Dependence of Slope for WSe_2-Ga Metal Contact

Metal-Semiconductor contact	**Temperature (K)**							
WSe_2-Ga	80	170	200	230	260	290	320	400
Slope	0.753×10^{-2}	0.787×10^{-2}	0.740×10^{-2}	0.782×10^{-2}	0.667×10^{-2}	0.566×10^{-2}	0.469×10^{-2}	0.223×10^{-2}

The analysis of WSe_2-Al Schottky Barrier diode shows that, with increase in temperature, the value of slope decreases. Similar to other metal-semiconductor Schottky barrier diodes, this diode also exhibits irregularity in the low temperature range, which can be found by including the tunneling and generation-recombination current in addition to the current due to thermionic emission. The final equation is the same as the one used in Case Studies 1 and 2 (Equation 7.1). Table 7.6 represents the temperature dependence of slope after considering the combined effect model and it can be concluded that the value of slope continuously decreases with increase in temperature irrespective of the metal used.

Table 7.6 Temperature dependence of slope for WSe_2– Ga metal contact after combined model effect

Metal-Semiconductor contact	Temperature (K)							
WSe_2-Ga	80	170	200	230	260	290	320	400
Slope	0.987×10^{-2}	0.927×10^{-2}	0.856×10^{-2}	0.782×10^{-2}	0.667×10^{-2}	0.566×10^{-2}	0.469×10^{-2}	0.223×10^{-2}

7.4 Case Study 4:WSe_2 - Gold Metal Contact

(a) Experimental Results

For the investigation of WSe_2/Au Schottky barrier junction, n-type WSe_2 single crystals were prepared by the chemical transport reaction technique in which $SeCl_4$ was used as transport agent. Gold electrodes were deposited by evaporation on the surface of WSe_2 crystal under vacuum (5×10^{-6} mbar). In addition, ohmic contacts were realized on the back of the sample using the eutectic mixture 25 mol% In- 75 mol% Ga. The electrical characterization of the interface has been performed using a frequency response analyzer Solartron 1170 (10^{-4} to 10^{6} Hz), and the C(V) measurements are done with a lock-in amplifier PAR124 [6].

General relationship of capacitance(C) with voltage(V) can be expressed as:

$$\frac{1}{C^2} = \frac{2(V_{bi}-V)}{q\varepsilon_s N_D} \qquad (7.2)$$

where, q is the charge; V_{bi} is the built-in potential; ε_s is the dielectric permittivity and N_D is the donor concentration

(b) Analysis

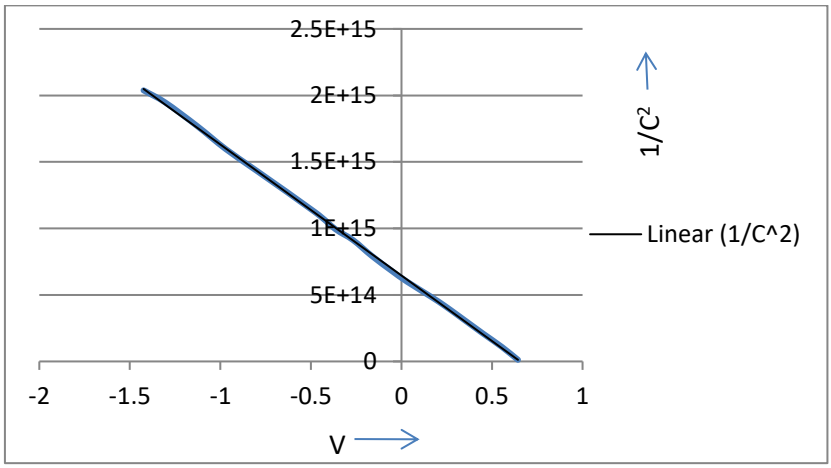

Figure 7.27 $1/C^2 = f(V)$ for (In-Ga)/WSe_2/Au sample at room temperature

Figure 7.27shows the $1/C^2 = f(V)$ characteristics obtained at room temperature for (In-Ga)/WSe_2/Au structure (sample area is 1 cm^2). It is also called the Mott-Schottky characteristics $1/C^2 = f(V)$. The sample that is used is the regular sample without any oxidation exposure.

From the graph above (Figure 7.27), the barrier height is deduced from the x-axis intercept of the $1/C^2$ versus V plot and the value obtained is 0.70 V. From this, another value for Schottky barrier height is obtained: $\phi_b^* = V_{fb} - kT \ln(N_a/N_c)$, resulting in 0.87 eV value (which is in agreement with the experimental results).

CHAPTER 8

APPLICATIONS OF WSe_2

In this chapter, a brief outline of applications of WSe_2 has been discussed. Due to the advances in fabrication methods such as exfoliation and synthetic techniques, it has been possible to fabricate ultra-thin monolayer TMDCs such as WSe_2. Due to their varying band gaps, they are reported to be used in applications such as transistors**,** solar cells, photodetectors, nanoelectronics, optoelectronics, etc.

8.1 Field Effect Transistors

The field-effect transistor (FET) is a transistor that uses an electric field to control the electrical behavior of the device. They are often called unipolar transistors because they involve single-carrier-type operation. FETs generally display very high input impedance at low frequencies. The conductivity between the drain and source terminals is controlled by the electric field in the device, generated by the voltage difference between the body and the gate of the device.

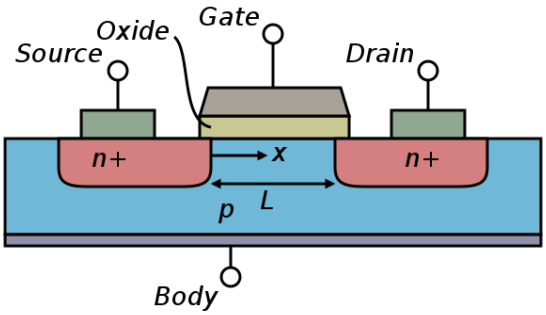

Figure 8.1 Cross section view of MOSFET.

Figure 8.1 shows a cross-section view of Metal Oxide Field Effect Transistor (MOSFET). They are basically used in logic gates due to their ON/OFF property.

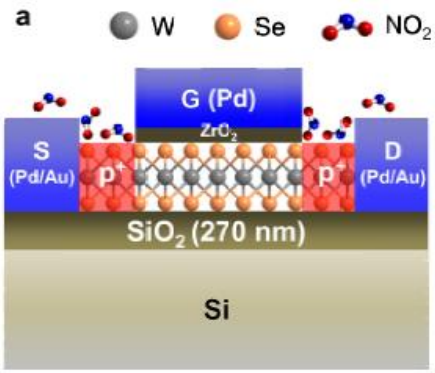

Figure 8.2 Schematic of a top-gated WSe_2 ML-FET, with chemically p-doped S/D contacts by NO_2 exposure.
Source: Fang H., et al., (2012). High-Performance Single Layered WSe_2 p-FETs with Chemically Doped Contacts, *ACS Publications,* 12, 3788-3792.

Figure 8.2 shows the schematic illustration of a top-gated WSe_2 ML-FET after NO_2source or drain (S/D) doping. The under-lapped regions are heavily p-doped, while the gate region remains near the intrinsic due to the protection of the active channel by the gate stack. Here the top-gate acts as the mask for protecting the active channel from NO_2 doping [29]. As per reports, these devices are high performance p-type field effect transistors.

8.1.1 High Gain Inverters Based on WSe_2 FETs

The most commonly utilized device configuration of TMDCs is Schottky barrier (SB) MOSFET structure, with WSe_2 being used because of its high valence band edge position which results in p-type operation. We achieve p-FETs by using high work function Pt contacts configured in a geometry of SB-MOSFET. On the other side, n-FETs are obtained by degenerate doping of the under-lapped contact regions. Such configuration provides us with a base to fabricate WSe_2Complementary MOS (CMOS) devices and logic gates. Schematics for the WSe_2 p- and n-FETs used is shown in Figure 8.3 (a) and (b) respectively.

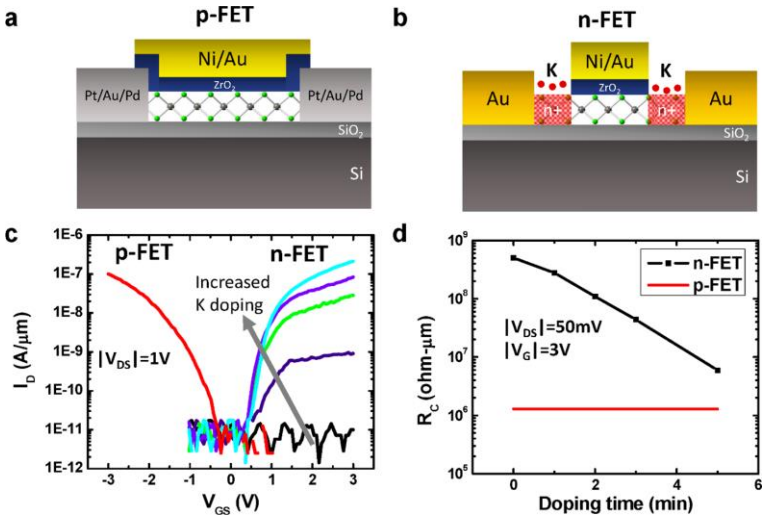

Figure 8.3 (a and b) Device schematics of the WSe_2 p- and n-FETs, respectively. (c)Transfer characteristics at V_{DS} = 1V of a WSe_2 p-FET and n-FET fabrication on the same flakes as a function of potassium doping time (1,2,3 and 5 min). (d)Extracted contact resistance, $R_{c'}$ as a function of K doping for p- and n-FETs.
Source: Tos un M., (2014). High-Gain Inverters Based on WSe_2 Complementary Field-Effect Transistors, *ACS Nano*, 8, 4948-4953.

Figure 8.3(c) shows the drain current, I_D, versus gate voltage, V_{GS}, curve at a drain voltage of V_{DS} = -1V for a WSe_2 p-FET fabricated on ~10 nm thick flake with Pt contacts. The channel length here is L= 2 μm and the gate electrode overlaps with the S/D contacts. The device exhibits clear p-type behavior with an ON/OFF current ratio of > 10^4 [14].

It can also be stated from the figure that the n-channel conduction increases as the doping time is increased due to the thinning of the SBs to the conduction band of WSe_2. Here, in the devices given, the contact resistances are large due to the Schottky like nature of the metal/WSe_2 interfaces for both p- and n-FETs.

From Figure 8.3(d), it is seen that the R_c of the p- and n-FETs as a function of K doping time is extracted by calculating the resistance at V_G = 3V from the transfer curves.

Table 8.1 Performance of FETs based on Multilayer WSe_2

Configuration (method)	Mobility ($cm^2 \cdot V^{-1} \cdot s^{-1}$)	On/Off Ratio	Sub-threshold Swing ($mV \cdot dec^{-1)}$	Temperature (K)	Reference
Four-terminal Top-gated	500(h)			300	[15]
Ionic Liquid Top-gated	200(e/h) 330(e)/270(h)	10		170/160/77	[15]
Back-gated (CVD)	350(h)	10^8		300	[15]
Back-gated (CVD)	650(h)	10^6	250/140	150/300/105	[15]
Back-gated (CVD)	10(h)	10^4		300	[15]
Back-gated	92(h)	10		300	[15]

Table 8.1 shows the tabular representation of performance of different FETs on multilayer WSe_2 prepared by mechanical exfoliation and by chemical vapor deposition. Here, in the table, the electron mobility is denoted by e and the hole mobility by h.

8.2 Optoelectronics

Tungsten diselenide exhibits unique complementary properties among all the TMDC materials. Monolayer WSe_2 has a large band gap of ~1.65 eV, while in bulk, it has a band gap of 1.2 eV [20]. Additionally, the transport properties of mechanically-exfoliated ML WSe_2 can be freely changed either to p-type behavior or ambipolar, depending on the type of contact metals. WSe_2 also has high absorption coefficient in the visible to infrared range, high quantum yield in photoluminescence (PL) and a good spin-orbit coupling (SOC). Considering all these advantages, a wide range of optoelectronic devices such as light emitting diodes, photodetectors and photovoltaic devices can be constructed using ML WSe_2.

It has high transparency, about 95%, which means it can simultaneously be used as window glass and as solar cell. The use of WSe_2 as photodiode is better, as the sensitivity of WSe_2 is one order of magnitude higher than that of graphene [20]. A Schottky junction, based on WSe_2, exhibits an energy conversion efficiency of 8.6% in a photovoltaic cell (PVC). Also, the efficiency of photo-electrochemical water splitting is reported to be above 14% [21].

As WSe_2has the lowest thermal conductivity among dense solids in disordered films of layered WSe_2 crystals, it may exhibit good applications in thermoelectric materials.

8.3 Quantum Performance

There has been both experimental and computational investigation on the effect of 2D materials including tungsten dichalcogenides in quantum Hall effect. WSe_2 quantum dots are utilized for integrated solid-state quantum photonics and processing of quantum information. After the investigation carried out by Chakraborty *et al.*, the possibility of using WSe_2 semiconductor as a host for quantum dot-like defects has increased. They display an excited-state lifetime of about 1 ns and an excitonic g-factor of 10 [21]. Koperski *et al.* report that, on contacting WSe_2 edge with Si/SiO_2 substrate, there are some centers which give rise to sharp emission lines of 100 μeV at low temperature range and thus act as single photon emitters [21].

8.4 Electrocatalysis

Doping can create a non-uniform charge distribution over the basal plane (bottom plane) making some sites catalytically active. Electrocatalysis is important to understand as it provides the involvement of these active sites due to the traceable electron transfer property. The most common electrocatalytic application of the TMDCs is for the Hydrogen evolution reaction (HER). Few scientists prepared a cobalt-doped WSe_2 which exhibited an excellent electrocatalytic property required for HER [21]. The mixing of cobalt with WSe_2 is not done physically as it results in poor electrocatalytic activity. The result is lack of dopant in the basal plane. As WSe_2 is composed of large sheets, activation of basal plane for the material to participate in the electrocatalysis is very important to achieve acceptable results.

Also, the role of conductive agent improves the electrocatalytic activity of WSe_2 toward HER. Substituting some of the Se atoms by S atoms (though the impact of carbon conductive agent is stronger) can create defects on the basal plane, which results in the required improvement.

Limitation: Though it has good results, the growth of WSe_2 remains poorly understood, because it is comparatively difficult to synthesize than MoS_2 (other TMDC).The reason is that the selenium precursors are less reactive than sulfur precursors [20].

CHAPTER 9

CONCLUSIONS

In the study presented above, the electrical properties of different metals on WSe_2 have been presented. The physical and electronic properties of bulk and monolayer WSe_2 have been studied and presented here based on literature survey.

The current-voltage characteristics have been discussed for WSe_2 Schottky barrier diode with different metal films. Using WebPlot Digitizer, the analysis of the current-voltage relationship dependence on temperature, in the range of 80 K to 400 K, shows that the current conduction is well within the domain of thermionic emission theory. From the analyzed graphs of I-V for In-pWSe_2, Al-pWSe_2 and Ga-pWSe_2, it is observed that, with increase in temperature, there is decrease in the slope, regardless of the metal being used. In the low temperature range, below 200K, an irregularity or discrepancy is observed, though there is a good linear fit in the high temperature range. These discrepancies imply that the current transport is not purely thermionic but has multiple charge conduction mechanisms in the low temperature regime. To avoid this irregularity, a combined effect model (or total current equation) has been considered in the study.

In the last part of the study, $1/C^2$ versus V for Au-nWSe_2, at room temperature, has been presented. From the analysis, the barrier height is found to be 0.70 V. This observed value is consistent with the experimental result obtained from the literature.

REFERENCES

1. Bobby A., et al, (2011). Schottky Barriers on Layered Anisotropic Semiconductor-WSe_2 -with 1000 Å Indium Metal Thickness, *Materials Sciences and Applications*, 2, 1000-1006.

2. Gary Hodes, (1989). Polyiodide-treated-n-WSe_2/Au Schottky junctions, *Applied Physics* Letters, 54, 2085-2087.

3. Wang Y., et al., (2016). Does p-type ohmic contact exist in WSe_2-metal interfaces?, *Nanoscale*, 8, 1179-1191.

4. Allain A., et al, (2014). Electron and Hole Mobilities in Single-Layer WSe_2, *ACS Nano*, 8, 7180-7185.

5. Klein A., et al., (1998). Photovoltaic properties of WSe_2 single-crystals studied by photoelectron spectroscopy, *Solar Energy Materials and Solar Cells*, 51, 181-191.

6. Bourezg R., et al, (1992). A study of the Au/WSe_2 interface, *Surface Science Letters*, 273, L419- L424.

7. Yang C., et al., (2017). Characters of group V and VII atoms doped WSe_2 monolayer, *J. Alloys and Compounds*, 699, 291-296.

8. Mathai A., et al, (2010). Schottky diode characteristics: Aluminum with 500 and 1000 Å thicknesses on p type WSe_2 crystal, *Wiley-VCH*, 7, 717-724.

9. http://www.mtixtl.com/xtlflyers/WSe2-P.pdf accessed on November 5, 2017.

10. https://arxiv.org/ftp/arxiv/papers/1212/1212.5415.pdf accessed on October 9, 2017.

11. Finteis Th., et al., (1997). Occupied and unoccupied electronic band structure of WSe_2, *Phy. Rev. B*, 55, 10400-10411.

12. astro1.panet.utoledo.edu/~relling2/.../20111025_lecture_4.2_phys4580.6280.pdf accessed on November 1, 2017.

13.courses.washington.edu/phys431/hall_effect/hall_effect.pdf accessed on October 25, 2017

14. Tosun M., et al, (2014). High-Gain Inverters Based on WSe_2 Complementary Field-Effect Transistors, *ACS Nano*, 8, 4948-4953.

15. Mingxiao Ye, et al, (2017). Recent Advances in Electronic and Optoelectronic Devices Based on Two-Dimensional Transition Metal Dichalcogenides, *Electronics*, 6, 1-40.

16. Zhao P., et al, (2014). Air Stable p-Doping of WSe_2 by Covalent Functionalization, *ACS Nano*, 8, 10808-10814.

17. Liu W., et al., (2013). Role of Metal Contacts in Designing High-Performance Monolayer n-type WSe_2 Field Effect Transistors, *ACS Publications*, 13, 1983-1990.

18. https://www.halbleiter.org/en/fundamentals/doping/ accessed on October 27, 2017.

19. Chen K., et al, (2014). Air stable n-doping of WSe_2 by silicon nitride thin films with tunable fixed charge density, *APL Materials*, 2, 092504- 092504-7.

20. https://arxiv.org/ftp/arxiv/papers/1505/1505.04706.pdf accessed on October 29, 2017.

21. Ali Eftekhari, (2017). Tungsten dichalcogenides (WS_2, WSe_2, and WTe_2): materials chemistry and applications, *J. Materials Chemistry A*, 5, 18299-18325.

22. Jager-Waldau A. and E. Bucher, (1991). WSe_2 Thin Films Prepared By Soft Selenization, *Thin Solid Films*, 200, 157-164.

23. https://ecee.colorado.edu/~bart/book/book accessed on July 05, 2017.

24. http://hyperphysics.phy-astr.gsu.edu/hbase/Tables/rstiv.html accessed on August 14, 2017.

25. https://public.wsu.edu/~pchemlab/documents/Work-functionvalues.pdf accessed on August 16, 2017.

26. Upadhyayula, et al, (1968). Semiconducting Properties of Single Crystals of n- and p-type Tungsten Diselenide (WSe_2), *J. Applied Physics*, 39, 353-358.

27. https://etda.libraries.psu.edu/files/final_submissions/9693 accessed on September 22, 2017.

28. Wei-Ting Hsu, et al, (2017). Evidence of indirect gap in monolayer WSe_2, *Nature Communications*, 8, 1-7.

29. Fang H., et al., (2012). High-Performance Single Layered WSe_2 p-FETs with Chemically Doped Contacts, *ACS Publications*, 12, 3788-3792.